Hyperexcitability of female serotonin neurons underlies sex-specific anxiety responses

Suzanne van der Veldt[1,2,3], Fiona Henderson[1,2,*], Lucia Pizzoccaro[1,2,*], Anne-Sophie Simard[1,2,#], Félix Perreault[1,2,#], Justine Fortin-Houde[1,2], Guillaume Ducharme[1], Bénédicte Amilhon[1,2]

[1] CHU Sainte-Justine Research Center, Montréal, Québec, Canada

[2] Département de Neurosciences, Université de Montréal, Montréal, Québec, Canada

[3] Current affiliation: Groningen Institute for Evolutionary Life Sciences, University of Groningen, the Netherlands

*equal contribution

#equal contribution

Corresponding author: Bénédicte Amilhon, benedicte.amilhon@umontreal.ca

Abstract

Mood disorders display robust sex differences in prevalence, symptom profile, and treatment outcomes, with women nearly twice as likely as men to be diagnosed. However, the neural substrates mediating sex-specific regulation of mood and related disorders remain incompletely understood. Here, we identify a neural circuit mechanism involving serotonergic (5-HT) projections from the median raphe region (MRR) to the ventral hippocampus (vHP) responsible for sex-specific regulation of anxiety-like behavior in mice. Using a multimodal approach combining electrophysiology, fiber photometry, and optogenetics, we show that 5-HT neurons targeting the vHP (5-HT^{vHP} neurons) display heightened intrinsic excitability and delayed deactivation in female mice during exposure to aversive environments. Optogenetic activation of this pathway enhanced anxiety-like behavior, and decreased risk-assessment behavior in females, but not in males. Collectively, our findings establish 5-HT^{vHP} neurons as a critical circuit for the regulation of anxiety and provide a mechanistic framework for understanding how serotonergic modulation contributes to sex-specific vulnerability to mood disorders.

Introduction

Mood disorders disproportionately affect women, who are not only more likely to be diagnosed, but also exhibit different symptom profiles and treatment responses compared to men[1,2]. Although this sex bias is well-documented, its neurobiological underpinnings remain poorly understood and largely understudied. Historically, the underrepresentation of female rodents in preclinical studies has limited our understanding of sex-specific mechanisms, partly due to incorrect assumptions about increased variability in female behavior[3]. Elucidating how biological sex influences mood and vulnerability to mood disorders at the neural circuit level is essential for developing more effective and equitable treatment strategies.

Anxiety disorders which are among the most prevalent mood-related conditions, show nearly a twofold higher incidence in women relative to men[2]. Drugs increasing serotonin (5-hydroxytryptamine, 5-HT) transmission remain first-line treatment for anxiety and related mood disorders, demonstrating the central role of 5-HT in the neurobiology of anxiety[4]. Yet, paradoxically, acute manipulations of 5-HT signaling, whether via pharmacology or optogenetic stimulation, have shown that increased serotonergic activity can exacerbate anxiety-like behavior in rodents[5–9]. These conflicting effects underscore the developmental, electrophysiological and functional heterogeneity of the 5-HT system[10,11], which comprises a diverse population of neurons distributed across multiple raphe nuclei, with widespread, frequently collateralized projections that collectively innervate the entire forebrain[5,12–16]. Moreover, multiple 5-HT receptors, some with opposing action, can be co-expressed in the same brain regions and neurons[17–21]. This complexity has long hampered our understanding of how serotonergic signalling regulates mood states.

Among the many targets of serotonergic cells, the ventral hippocampus (vHP), a core component of the limbic system, stands out as a critical node in the regulation of anxiety and behavioral inhibition[22–25]. The vHP shares connections with the lateral septum, prefrontal cortex (PFC), lateral hypothalamus and raphe, circuits previously described for their role in anxiety processing[26–32]. Lesions of the vHP consistently produce anxiolytic effects[22,25]. vHP pyramidal cells and interneurons represent aversive and potentially threatening environments[26,28,31,33–35] and manipulation of vHP activity or outputs modulates anxiety-like behaviors in rodents[26,27,32,35,36]. In humans, reductions in anterior hippocampal volume are observed in individuals with anxiety disorders[37], and the anterior hippocampus is engaged during approach-avoidance behaviors[38,39], reinforcing the conserved role of this structure in anxiety regulation across species.

The median raphe region (MRR), comprising the median raphe nucleus (MnR) and the paramedian raphe (PMnR), is the main source of serotonergic inputs to the hippocampus in mice[14]. Although comparatively less explored than the dorsal raphe nucleus[10,40–43], growing evidence highlights the MRR as a key group of 5-HT neurons with roles in aversion, avoidance and more[44–50]. While the impacts of 5-HT release on dorsal hippocampus (dHP) activity and functions have been documented[8,21,51–56], effects of 5-HT on the vHP have received less attention. Altered 5-HT transmission in the vHP[9,57] enhances anxiety-related behaviors, suggesting a critical pathway for 5-HT-mediated

regulation of anxiety states[9,57–59]. The involvement of this pathway, and the extent to which sex-specific differences in vHP-projecting 5-HT neurons (5-HT^{vHP} neurons) from the MRR contribute to anxiety regulation, await clarification.

This study aims to advance understanding of how serotonergic circuits contribute to the sex disparity in mood disorders. We postulate that 5-HT^{vHP} neurons are a central component of the neural circuits governing anxiety. To test this hypothesis, we use a combination of circuit-specific fiber photometry, electrophysiology, optogenetics and behavioral analysis. We show that these neurons exhibit heightened intrinsic excitability, spontaneous activity and increased *in vivo* recruitment in females. These sex differences translate into circuit- and behavior-specific consequences: 5-HT^{vHP} neurons in females exhibit delayed disengagement from aversive contexts, selectively alter hippocampal theta dynamics during novelty exposure, and promote anxiety-like behavior, increased risk-assessment, and grooming when optogenetically activated. Together, our findings delineate a circuit-specific mechanism by which serotonergic signalling in the vHP contributes to sexually divergent anxiety responses, offering insights in how sex differences at the cellular and circuit level may underlie vulnerability to mood disorders.

Results

5-HT^{vHP} neurons in the MRR display sex-specific activity dynamics in the elevated plus maze.
The MRR is the primary source of 5-HT inputs to the vHP in mice[14] and has been implicated in the response to aversive stimuli[46,47]. Notably, the MRR receives direct input from the lateral habenula (LHb), a core structure in aversion-related circuits that signals negative motivational value and modulates serotonergic systems[48,60–62]. We hypothesized that exploration of a novel and potentially threatening environment would engage 5-HT^{vHP} neurons.

We used the elevated plus maze (EPM), a classical anxiety assay that reliably elicits approach-avoidance conflict behaviors in both male and female mice[63]. Prior work has shown that EPM exploration globally increases 5-HT levels in the vHP, as measured over slow time scales with microdialysis[57,64]. To monitor circuit-level activity with greater temporal precision, we selectively recorded activity of MRR 5-HT^{vHP} neurons using *in vivo* fiber photometry in freely moving SERT-Cre mice. A retrogradely transported AAV encoding the calcium (Ca^{2+}) indicator GCaMP6s was bilaterally infused in the vHP, enabling selective monitoring of Ca^{2+} dynamics in 5-HT^{vHP} neurons (Fig. 1a). Fiber placement and viral expression were histologically confirmed to target MRR (Fig. 1b, Extended Data Fig. 1a). GCaMP6s expression was highly specific to 5-HT neurons, with 99.86% of GCaMP6s-expressing cells in the raphe co-expressing the selective 5-HT neuron marker tryptophan hydroxylase 2 (Tph2, n = 2 mice, 709 neurons, data not shown).

We tracked mouse movements and identified locomotor epochs corresponding to transitions from closed arms ("safer" zones) to open arms (aversive zones) of the EPM (Fig 1d), or transitions restricted to the closed arms (Fig. 1f). Closed-to-open epochs were defined as the mouse spending minimally 10 s in a closed arm before exploring center/open arms for at least 2 s. Closed-to-closed

epochs were defined as transitions between closed arms with a maximum of 1 s spent in the center. Changes in fluorescence were averaged and aligned to the timepoint where center-of-body marker crossed the closed arm-center limit.

In both sexes and trajectories, 5-HT^{vHP} population activity peaked around transitions (Fig. 1c-d,f). We observed similar transient increases in 5-HT^{vHP} population activity when mice initiated high velocity locomotion bouts in the EPM, independent of location in the maze, or in the open field (OF) (Extended Data Fig. 1b-i). Velocity and area under the curve (AUC) of fluorescence signal during 1 s surrounding the locomotion onset did not differ between sexes. Consistent with previous evidence[47,65,66], these results indicate that 5-HT^{vHP} neurons are engaged during locomotion.

Transitions from closed arms into the aversive open compartments were associated with a ramping increase of 5-HT^{vHP} population activity in both sexes (Fig. 1d,e), suggesting progressive recruitment of this population prior to open-arm entry. By contrast, 5-HT^{vHP} activity remained stable before transitions between closed arms (Fig. 1f,g). We also focused more closely on 5-HT^{vHP} activity around transitions in and out of the “safer” closed arms of the EPM. When mice retreated from center/open arms back into the closed areas (≥ 2 s in the center/open followed by ≥ 2 s in closed) activity of 5-HT^{vHP} neurons decreased in both sexes; however, this reduction was significantly attenuated in females (Fig. 1h-j), despite comparable velocities (Fig. 1k-l). These results suggest that 5-HT^{vHP} population activity remains elevated in females upon return to a less aversive environment, indicating a sex difference in how this circuit disengages from anxiogenic contexts. Conversely, exiting the closed arms did not lead to a subsequent change in 5-HT^{vHP} population activity, and no differences between males and females were observed (Fig. 1m-p).

During EPM exploration, locomotor activity typically declines over time, likely reflecting habituation as animals become familiar with the environment[67,68]. We therefore examined how the decrease in activity of 5-HT^{vHP} neurons during closed arms retreats evolved over the duration of the test. Specifically, we correlated AUC of the calcium signal during the 1 to 2 second period following closed arm entry (as in Fig. 1i) with elapsed time in the EPM for both female and male mice. In males, the decrease in 5-HT^{vHP} neurons population activity remained stable across the session (see example correlation Fig. 1q, right). In contrast, in females, this suppression correlated with time (see example correlation Fig. 1q, left): during the early phases of the test, 5-HT^{vHP} neuron activity remained high upon retreat into a closed arm, but a reduction gradually emerged as the session progressed and animals habituated to the test apparatus. Changes in AUC over time were quantified by subtracting the retreat-related response in the last 10 min of the EPM to response in the first 10 min (Fig. 1r). While activity of MRR 5-HT^{vHP} neurons remained stable in male mice, post-retreat responses in females evolved with time (Fig. 1r,s) showing that during early exploration of the EPM, female 5-HT^{vHP} neurons maintain elevated activity upon retreat into less aversive compartments of the maze. Together, these findings indicate that 5-HT^{vHP} neurons exhibit sex-specific activity dynamics during exploration and habituation in the EPM.

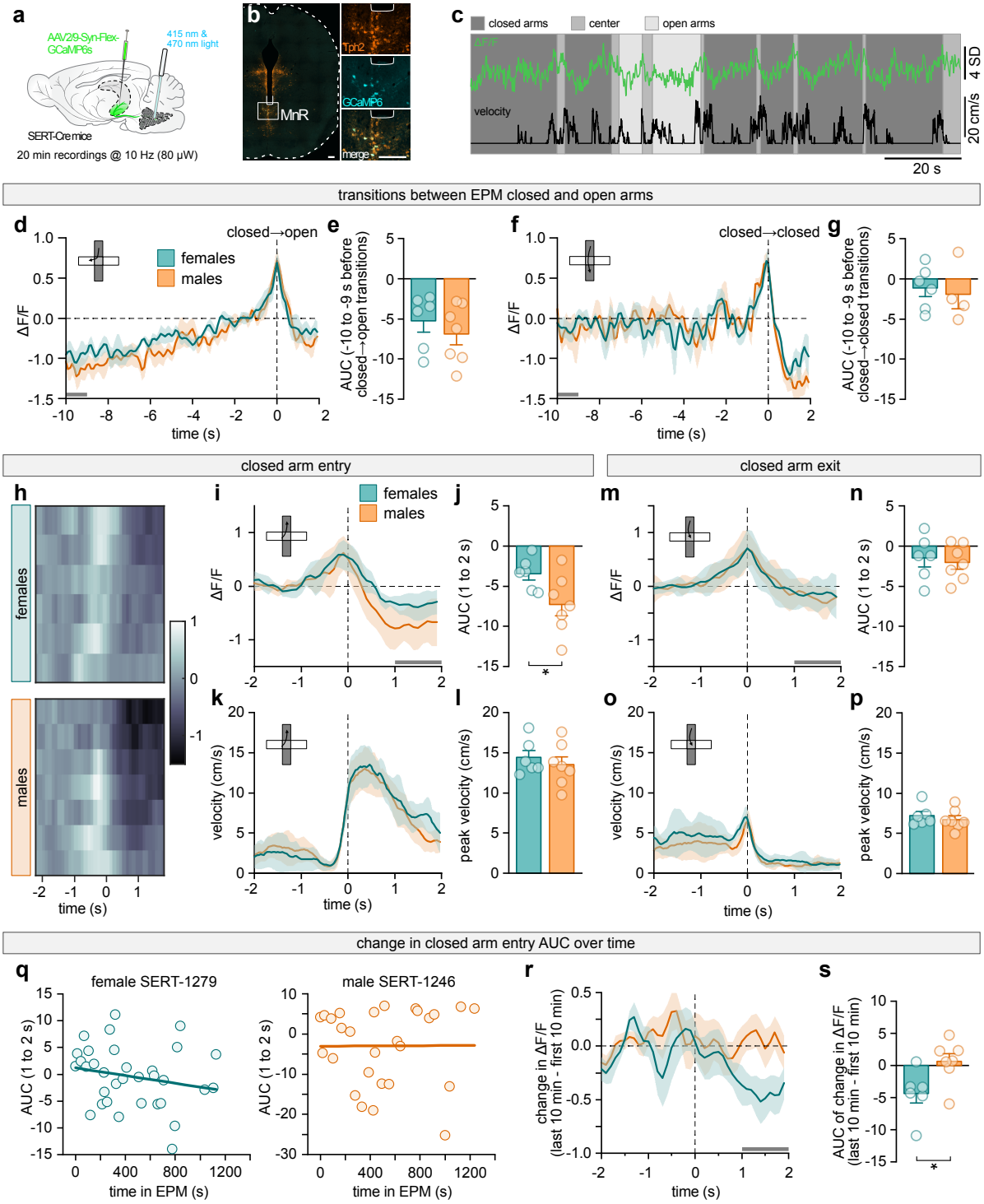

Figure 1: Female 5-HT^{vHP} neurons exhibit delayed disengagement from an aversive context. a, Schematic of experimental configuration: a retrograde AAV containing the Cre-dependent calcium indicator GCaMP6s was infused bilaterally in the vHP of SERT-Cre mice. 5-HT^{vHP} population activity was recorded using an optic fiber implanted above the MRR. **b,** Example fiber placement above the MRR, with magnified view of cell bodies (right). 5-HT neurons (Tph2+) are shown in orange; GCaMP6s-labelled 5-HT^{vHP} neurons shown in cyan. Scale bars = 200 µm. **c,** Example ΔF/F (green) and velocity (black) traces in the EPM. Shaded epochs indicate maze location: closed arms (dark gray), center (medium gray) and open arms (light gray). **d,** Mean normalized ΔF/F aligned to transitions from a closed arm to an open arm for females (teal, n = 6) and males (orange, n= 7). Dotted vertical line indicates timepoint where center-of-body marker crossed the center-closed arm limit. Gray bar indicates the time window used for panel **e**.

e, Area under the curve (AUC) of ΔF/F obtained over 10 - 9 s preceding closed arm exit (gray bar in **d**). **f,** Same as **d**, but for closed→closed arm transitions. Dotted vertical line indicates timepoint where center-of-body marker crossed the closed-arm center limit exiting the first closed arm. Gray bar indicates the time window used for panel **g**. **g,** AUC of ΔF/F obtained over 10 - 9 s preceding transition timepoint (gray bar in **f**). **h,** Mean ΔF/F for closed arm entries from center/open zones for each female (top, n = 6) and each male (bottom, n = 7). **i,** Mean normalized ΔF/F for closed arm entries from center/open zones for females (teal, n = 6) and males (orange, n = 7). Dotted vertical line indicates timepoint where center-of-body marker crossed the center-closed arm limit. Gray bar indicates the period used for panel **j**. **j,** AUC of ΔF/F obtained over 1 - 2 s after closed arm entry (gray bar in **i**). Two-sample t-test, P = 0.0430. **k,** Velocity around closed arm entries for females (teal, n = 6) and males (orange, n = 7). **l,** Peak velocity quantification (-0.5 to 0.5 s) for females (teal, n = 6) and males (orange, n = 7). **m – p,** Same as in **i** – **l** but for closed arm exits. **q,** AUC of ΔF/F obtained over 1 - 2 s after each closed arm entry as a function of time spent in the EPM for a representative female (left) and male (right). **r,** Change in mean ΔF/F (last 10 min – first 10 min) after closed arm entry (1 - 2 s) for females (teal, n = 6) and males (orange, n = 7). Dotted vertical line indicates timepoint where center-of-body marker crossed into the closed arm. Gray bar indicates the period used for panel **s**. **s,** Corresponding AUC quantification of change in ΔF/F for period indicated by gray bar in **r**. Two-sample t-test, P = 0.0284. All data are mean ± s.e.m; * : P < 0.05. For detailed statistical information, see Extended Data Table 1.

Hippocampal response to novelty is modulated by 5-HT selectively in female mice.

Approach-avoidance conflict behaviors arise from competing drives to explore novelty and avoid aversive features[69], a pattern readily observed in the EPM. We hypothesized that the sex-specific dynamics of MRR 5-HT^{vHP} neuron activity might partly reflect a delayed familiarization to the novel environment in females, and next interrogated the roles of 5-HT^{vHP} neurons in modulating the response to novelty.

To measure the hippocampal response to novelty and its modulation by 5-HT we turned to local field potentials (LFP) and optogenetics. Theta oscillations (6-10Hz) dominate hippocampus LFP when mice are exploring an environment[70–72]. Theta exhibits a well-established linear relationship with locomotion, with increased speed being accompanied by higher theta frequency[73–76]. Prior work shows that exposure to a novel environment robustly modulates two properties of the speed-theta frequency correlation: the slope of the linear frequency-speed relationship ("slope") and its y-axis intercept ("intercept")[77].The slope is a metric known to be modulated by novelty on a timescale of minutes in the dHP, with flatter slopes observed in novel environments; as animals habituate, the slope progressively steepens[75,77,78]. In contrast, the intercept is sensitive to anxiolytic drugs, which consistently decrease intercept values independent of their mechanism of action[79]. We therefore examined whether activation of 5-HT^{vHP} neurons modulates these novelty- and anxiety-related theta dynamics in males and females.

We expressed an excitatory opsin, ChETA, or a control eYFP construct in 5-HT^{vHP} neurons (Fig. 2a-d). ChETA expression was highly specific to 5-HT neurons, with only 0.21 ± 0.11% of ChETA-expressing neurons lacking Tph2 co-expression. Transfected neurons were similarly distributed across multiple raphe subregions for males and females, with labeled neurons primarily located in the B9 cell group, the MRR and the interfascicular part of the DR (DRI; Fig. 2b,c; Extended Data Fig. 2). Importantly, the proportion of 5-HT cells retrogradely labeled from the vHP was similar between males and females, representing in % of 5-HT neurons: 17.91 and 18.90 in B9, 14.36 and 19.24 in the MRR, and 15.18 and 20.33 in the DRI, in females and males respectively (Fig. 2c; Extended Data Fig. 2b-c).

Using an optic fiber placed above the labeled population, 5-HT^{vHP} neurons were activated while recording LFP simultaneously from the vHP and dHP (Fig. 2d,f; Extended Data Fig. 3). Recordings were conducted during free exploration of a novel environment with low-threat characteristics: a small

open field in low lighting conditions (40 cm length, 70±5 lux), designed to minimize aversive features such as bright illumination and open space. LFP were recorded across baseline and stimulation (20 Hz) epochs (Fig. 2e). As expected, dHP theta frequency linearly scaled with running speed. In eYFP controls the slope of this relationship increased from the first 4 minutes of exploration (baseline, grey lines), to the subsequent 4 minutes (stimulation epoch, blue lines) in both females and males (Fig. 2g,h). A similar pattern was observed in the vHP (Fig. 2k,l). Photoactivation of 5-HT^{vHP} neurons had sex-specific effects on the modulation of hippocampal novelty response. In male ChETA mice, the slope increase during stimulation was similar to eYFP controls (Fig. 2j,n,o,q). In contrast, female ChETA mice failed to show the slope increase normally observed as the novelty of the environement decreases, for both dHP (Fig. 2i,o) and vHP recorded theta (Fig. 2m,q). Thus, 5-HT^{vHP} neurons influence the habituation-related change in slope of hippocampal theta frequency-velocity relationship in a sex-specific manner.

Moreover, theta frequency at intercept, a metric modulated by anxiolysis, was also affected by 5-HT^{vHP} neuron activation in a sex-specific manner. In males, the change in intercept over time was similar between eYFP controls and ChETA groups in both dHP (Fig. 2p) and vHP (Fig. 2r). By contrast, photoactivation of 5-HT^{vHP} neurons prevented the decrease in intercept observed in female eYFP mice, in both the dHP (Fig. 2p) and the vHP (Fig. 2r), suggesting a sex specific effect of increasing 5-HT^{vHP} neuron activity on anxiety levels. Taken together, these findings show that 5-HT^{vHP} neurons selectively influence theta oscillations properties underlying novelty processing and anxiety-related behavior in a sex-dependent fashion.

Using double retrograde tracing we confirmed that, under our experimental conditions, a subset of 5-HT^{vHP} neurons also innervate the dHP, likely contributing to the similar modulation of theta oscillations observed in both dHP and vHP during 5-HT^{vHP} activation (Extended Data Fig. 4). To control for the absence of altered locomotor behavior, we quantified movement across stimulation conditions in mice implanted with only optic fibers (Extended Data Fig. 5a). Importantly, optogenetically evoked changes in hippocampal theta occur independently of gross locomotor changes in females (Extended Data Fig. 6), consistent with prior reports that DR, but not MnR, 5-HT neurons modulate rodent locomotion[8,80–82].

Altogether, these findings demonstrate that, in a novel and low-threat environment, 5-HT^{vHP} neurons shape circuit-level signatures of novelty in a sex-dependent fashion, without prominent influence on locomotion. In addition, sex-specific changes in the intercept of the speed-theta frequency relationship suggest that increased 5-HT^{vHP} neurons activity modulates anxiety levels predominantly in females. To test whether increased serotonergic tone in the vHP modulates anxiety-related behaviors, we assessed the impact of their activation in classical anxiety tests.

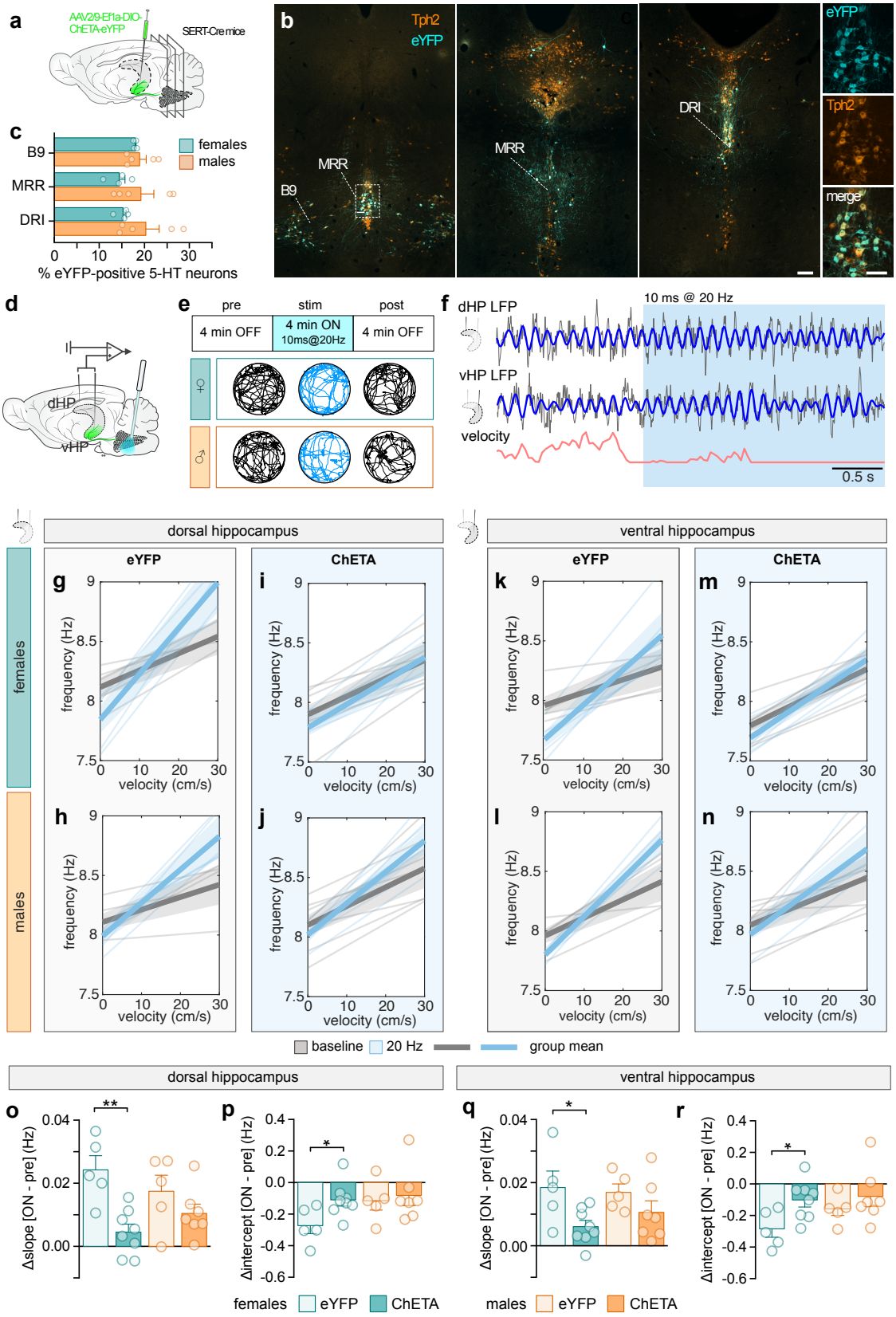

Figure 2: Activation of 5-HT^{vHP} neurons disrupts theta-velocity relationship selectively in females. a, Schematic of experimental configuration: a retrograde AAV containing Cre-dependent construct eYFP was bilaterally infused into the vHP of SERT-cre mice. **b,** Representative coronal sections showing eYFP-labeled neurons in the

B9, MRR and DRI regions at different anteroposterior levels. 5-HT+ cells are detected using Tph2 immunostaining. Scale bars = 200 µm (overviews**),** 100 µm (magnified). **c,** Percentage of eYFP+ 5-HT neurons in raphe of females (teal, n = 4 mice) and males (orange, n = 4 mice). **d,** Schematic of simultaneous multi-site local field potential recording with pathway specific optogenetic stimulation. **e,** Stimulation paradigm and example trajectories for a female (top) and male (bottom) animal for baseline (pre) and stimulation (stim) period. **f,** Example raw LFP traces (gray) recorded from dHP (top) and vHP (middle) and corresponding velocity (bottom), for animals exploring the open field, 2.5 s before and after stimulation onset. Blue: theta filtered traces. Red: instantaneous animal velocity. **g – n,** Instantaneous theta frequency as a function of running speed, for dHP (**g-j**) and vHP (**k-n**) for pre (gray) and stimulation (blue) epochs for female-eYFP (n = 5, **g,k**), male-eYFP (n = 5, **h,l**), female-ChETA (n = 8, **i,m**) and male-ChETA (n = 7, **j,n**). Thin lines: individual animals; thick lines: group mean. Shaded areas represent s.e.m. **o,** For the dHP, difference between slopes during optogenetic stimulation and baseline epochs**.** Two sample t-test: females (ChETA vs control), $P = 0.0016$. **p,** For the dHP, difference between intercepts during optogenetic stimulation and baseline epochs. Two-sample t-test: females (ChETA vs control), $P = 0.0278$. **q,** Same as o, for vHP. Two sample t-test: females (ChETA vs control), $P = 0.0251$. **r,** Same as p, for vHP. Two sample t-test: females (ChETA vs control). $P = 0.0228$. All data are shown as mean ± s.e.m; * : $P < 0.05$, ** : $P < 0.01$; dHP: dorsal hippocampus; eYFP: enhanced yellow fluorescent protein; Tph2: tryptophan hydroxylase 2; vHP: ventral hippocampus. For detailed statistical information, see Extended Data Table 1.

Optogenetic activation of 5-HT^{vHP} neurons promotes anxiety-like behavior and decreases risk-assessment in females.

The MnR has previously been implicated in the regulation of anxiety behavior[44,80,83], and females show higher anxiety than males across species[1,2,84]. Our fiber photometry data indicate that female 5-HT^{vHP} neurons disengage more slowly from aversive contexts. Activation of this pathway attenuates the normal vHP and dHP activity changes associated with familiarization during exploration of a new environment. We next tested whether stimulating this pathway would produce corresponding changes in anxiety-like and risk assessment behaviors.

To assess the functional consequences of selective activation of 5-HT^{vHP} neurons during ethologically relevant anxiety assays, we used the same cohorts of male and female mice previously tested for locomotor effects of stimulation (Extended Data Fig. 5). Each cohort was tested by experimenters of opposite sex, and analyzed by three-way ANOVA to control for effect of cohort, sex and stimulation (Extended Data Table 1, see methods; Extended Data Fig. 6). Light was delivered to the raphe during subsequent exposures to the EPM and the successive alleys (SA) tasks (Fig. 3a,b). In the EPM, activation of 5-HT^{vHP} neurons increased time spent in the closed arms in female ChETA mice as compared to both female eYFP controls and male ChETA mice (Fig. 3c, Extended Data Fig. 6a,b,c). Likewise during activation, female ChETA mice made fewer open arm entries than both same-sex eYFP controls and male ChETA mice (Fig. 3d), consistent with increased anxiety-like behavior. These sex-specific anxiogenic effects were also evident in the SA task. Activation of 5-HT^{vHP} neurons reduced exploration of aversive zones in female ChETA mice, as reflected by higher occupancy scores (Fig. 3e, see methods) and fewer entries in the open alleys (Fig. 3f), compared to both female eYFP controls and male ChETA mice. Importantly, these behavioral changes occurred largely independent of alterations in gross locomotor activity. In the EPM, optogenetic stimulation did not significantly affect distance traveled (Extended Data Fig. 5i). In the SA task, however, stimulation of 5-HT^{vHP} neurons significantly reduced distance traveled in female ChETA animals compared to male ChETA mice (Extended Data Fig. 5j), consistent with increased avoidance.

We hypothesized that if reduced exploration of the open arm in the EPM or the open zone in the SA by female ChETA mice reflected heightened anxiety, rather than a general decrease in exploratory drive, it would be accompanied by a reduction in risk assessment behaviors. Head dipping, an exploratory behavior in which the animal lowers its head over the edge of an open arm, was decreased upon stimulation of 5-HT^{vHP} neurons in female ChETA mice in the EPM (Fig. 3g). Stretch-attend postures, where mice elongate their bodies in a low stance to cautiously assess their environment, were also strongly reduced in female ChETA animals in the EPM (Fig. 3h). This pattern was replicated in the SA, where optogenetic activation similarly reduced both head dipping (Fig. 3i) and stretch-attend postures (Fig. 3j) in female ChETA mice compared to eYFP controls. Together, these findings indicate that activation of 5-HT^{vHP} neurons enhances anxiety-like states in females, suppressing risk-assessment behaviors characteristic of approach-avoidance conflict, rather than merely reducing overall exploratory drive.

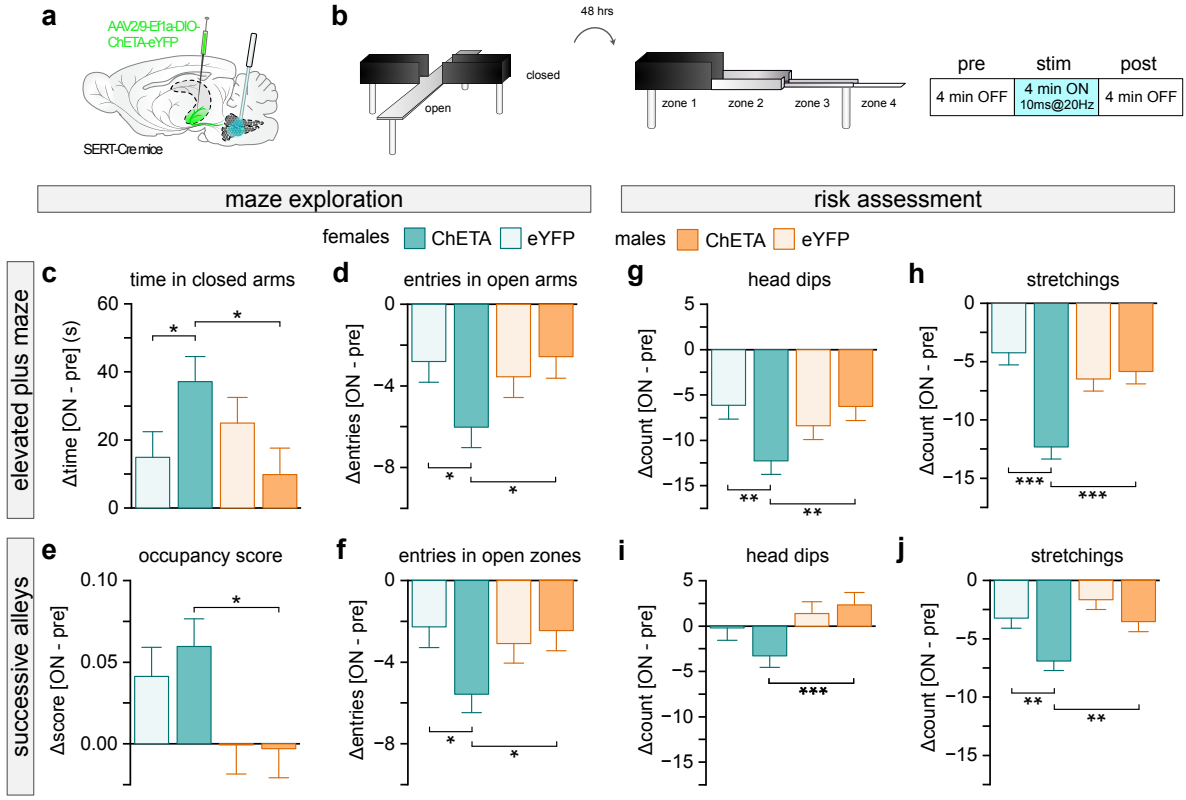

Figure 3: 5-HT^{vHP} activation increases anxiety-like behaviors and decreases risk assessment selectively in females. a, Schematic of experimental configuration: a retrograde AAV containing Cre-dependent excitatory opsin ChETA or YFP control is bilaterally infused in the vHP of SERT-Cre mice of both sexes and an optic fiber is implanted above the MRR region. **b,** Experimental set up: EPM (left) and SA (middle) experiments, with optogenetic stimulation paradigm (right). **c-j**, Change (stim – pre) in behavioral measures during EPM and SA testing. Data are from two independent experiments and analyzed by three-way ANOVA with Holm's multiple comparison testing. Significant comparisons are reported as *P* values. **c**, time in closed arms of the EPM: females (ChETA vs control), $P = 0.0378$; ChETA (female vs male), $P = 0.0126$. **d,** open arm entries of the EPM: females (ChETA vs control), $P = 0.0278$; ChETA (female vs male). $P = 0.0204$. **e,** anxiety score (see methods) in the SA: ChETA (female vs male), $P = 0.0134$.

f, number of open zone (zone 2, 3 and 4) entries: females (ChETA vs control), $P = 0.0182$; ChETA (female vs male), $P = 0.0237$. **g,** number of head dips in the EPM: females (ChETA vs control), $P = 0.0052$; ChETA (female vs male), $P = 0.0068$. **h,** number of stretchings in the EPM: females (ChETA vs control), $P < 0.0001$; ChETA (female vs male), $P < 0.0001$. **i,** number of head dips in the SA: ChETA (female vs male), $P = 0.0009$. **j**, number of head dips in the SA: females (ChETA vs control), $P = 0.0026$; ChETA (female vs male), $P = 0.0039$. Data are shown as mean ± s.e.m. * : $P < 0.05$, ** : $P < 0.01$. For detailed statistical information and for the numbers of male and female mice used, see Extended Data Table 1. For an overview of all behavioral variables analyzed, see Extended Data Table 2.

Activation of 5-HT^{vHP} neurons promotes anxiety-related grooming in females.

Self-grooming is increasingly recognized as a displacement behavior indicative of elevated stress and conflict, as well as a translationally relevant readout of affective states[85–87]. Under conditions of heightened arousal, grooming can serve as an adaptive coping strategy[88]. To directly assess 5-HT^{vHP} neuronal dynamics related to grooming under anxiogenic conditions, we used fiber photometry to align population activity to onset and end of grooming bouts in the EPM. Activity of 5-HT^{vHP} closely tracked grooming behavior (Fig. 4a): whereas transitions from closed to open arms were associated with a ramping increase in 5-HT^{vHP} neurons activity (Fig. 1), grooming episodes coincided with an immediate reduction in calcium signal in both sexes (Fig. 4b). Population activity returned upon grooming termination (Fig. 4c), consistent with the idea that grooming acts as a transient strategy to downregulate heightened serotonergic activity. Quantification of event-aligned fluorescence revealed no significant sex differences in activity dynamics, either during the first 5 seconds of grooming initiation (Fig. 4f) or in the 5-second periods following termination (Fig. 4g). Grooming bouts were predominantly surrounded by low locomotor activity (<5cm/s) in both males and females (Fig. 4d,e), indicating that increased 5-HT^{vHP} activity following grooming likely reflects the resumption of exploration. This suggests that grooming may serve as an alternative strategy to downregulate heightened serotonergic activity, consistent with its role as a displacement behavior under conditions of conflict or arousal.

We then tested whether optogenetic activation of 5-HT^{vHP} neurons was sufficient to alter grooming behavior across different environments. During EPM and SA exploration, both anxiogenic contexts, optogenetic activation produced a robust increase in time spent grooming selectively in female ChETA mice relative to female eYFP controls and male ChETA mice (Fig. 3h,i; Extended Data Fig. 6d,e,f), as well as number of grooming episodes and total grooming duration (Extended Data Table 1). In contrast, during low-threat open field exploration, stimulation did not significantly affect grooming duration in either sex (Fig. 4j, Extended Data Table 1). These findings indicate that vHP-projecting serotonergic neurons contribute to the expression of stress-related grooming in a sex- and context-dependent manner. The absence of effects in the open field suggests that elevated environmental threat is necessary for this circuit to drive displacement-like behaviors.

Because serotonergic axons form extensive collaterals[15], we next asked whether off-target effects via collateral projections could contribute to the observed behavioral changes. Using eYFP labeling of 5-HT^{vHP} neurons, we mapped their axonal distribution and confirmed collateral innervation across several regions, including the dHP, lateral and medial septum and prefrontal cortex (Extended Data Fig. 7). We observed no sex differences in the pattern or density of these collateral projections, suggesting that the sex-specific behavioral effects are unlikely to arise from differential collateralization between the sexes.

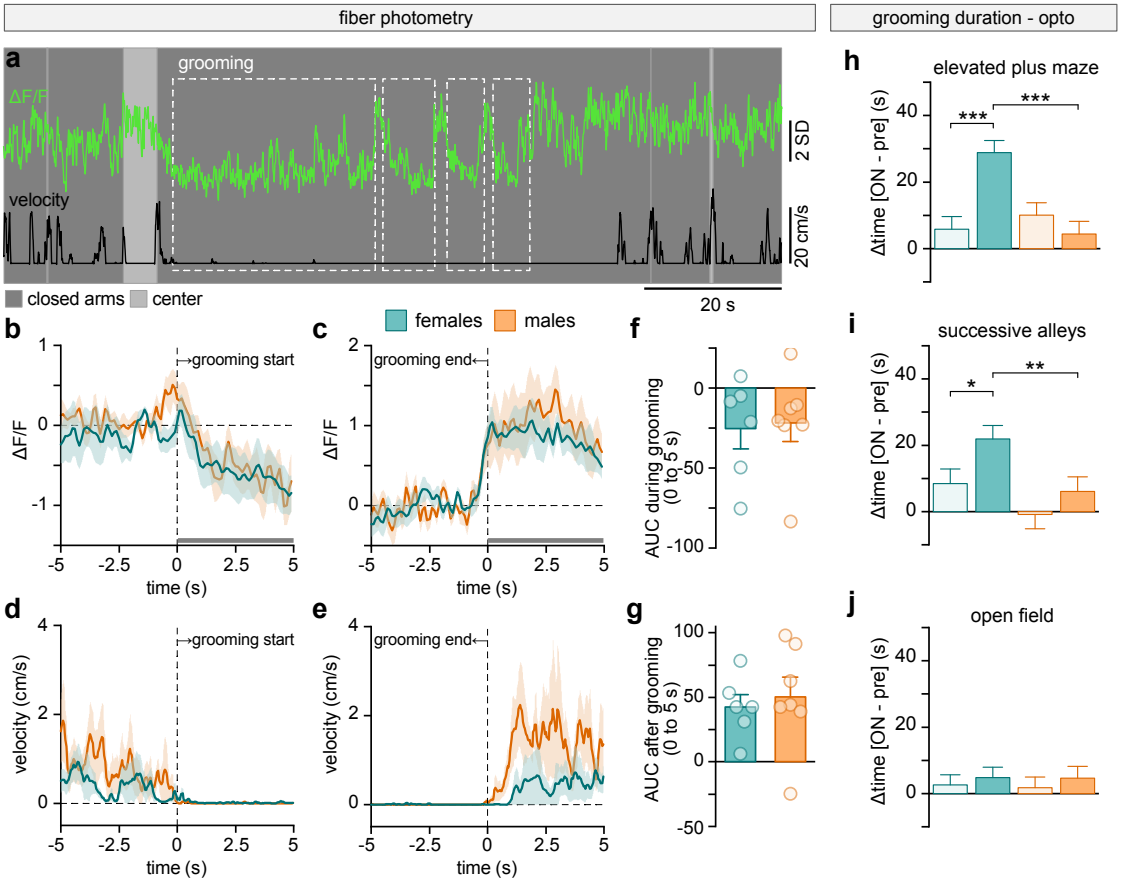

Figure 4: Activation of 5-HT^{vHP} neurons increases grooming in a context-dependent manner. a, Example 5-HT^{vHP} Ca^{2+} ΔF/F (green) over time, with locomotion velocity (black) during EPM exploration. **b – c,** ΔF/F aligned to grooming onset (**b**) and end (**c**) as indicated by vertical dotted line, for females (teal, n = 6) and males (orange, n = 7). **d,** Locomotor velocity for the same animals aligned to start and **e** end of grooming bouts. **f – g,** Quantification of the AUC for 0 - 5 s of panel **b** after grooming onset (**f** and of panel **c** after grooming offset (**g**). **h,** Change in total grooming time (stim – pre) in the EPM. Three-way ANOVA with Holms multiple comparison testing: females (ChETA vs control), P = < 0.0001; ChETA (female vs male), P < 0.0001. **i,** Same as **h**, but in the SA. Three-way ANOVA with Holms multiple comparison testing: females (ChETA vs control), P = 0.0316; ChETA (female vs male), P = 0.0098. **j,** Same as **i**, but in the open field. Data are shown as mean ± s.e.m. * : P < 0.05, ** : P < 0.01; For **h-j**, data are from two independent experiments and were analyzed by three-way ANOVA. For detailed statistical information and for the numbers of male and female mice used, see Extended Data Table 1. For an overview of all behavioral variables analyzed, see Extended Data Table 2.

MRR 5-HT^{vHP} neurons are more excitable in female mice.

To understand the cellular basis of these sex-specific behavioral effects, we next examined whether 5-HT^{vHP} neurons differ in their intrinsic electrophysiological properties. We performed whole-cell patch-clamp recordings in acute brain slices from retrogradely labeled cells in the B9, MRR and DRI from male and female mice (Fig. 5, Extended Data Fig. 8). In the B9, no sex differences were observed in firing frequency (Fig. 5a-c), resting membrane potential (RMP, Fig. 5d), input resistance (Fig. 5e), or spike frequency adaptation during sustained activation, quantified by the adaptation index (Fig. 5f, see methods). In contrast, 5-HT^{vHP} neurons in the MRR from female mice exhibited consistently higher firing rates across all depolarizing current steps (Fig. 5g-i) and a more depolarized RMP compared to males (Fig. 5j). Notably, these neurons showed a significantly reduced adaptation index compared to males (Fig. 5l). The absence of differences in input resistance (Fig. 5j) suggests that sex differences in

excitability are not due to changes in passive membrane properties. In turn, 5-HT^{vHP} neurons in the DRI showed comparable firing frequency between sexes (Fig. 5m-o) but, similarly to observations in the MRR, their RMP was more depolarized in female mice (Fig. 5p). No differences between sexes were found for DRI 5-HT^{vHP} neurons input resistance (Fig. 5q) or adaptation index (Fig. 5r). Notably, the firing frequencies of female MRR 5-HT^{vHP} neurons were the highest among all regions and sexes (Extended Data Fig. 8c). Moreover, under baseline conditions, 29% of female MRR 5-HT^{vHP} neurons (5/17 cells) exhibited spontaneous firing, which was not observed in any neuron recorded from the B9 and DRI regions in either sex, or in male MRR 5-HT^{vHP} neurons.

We next asked whether these intrinsic electrophysiological differences translate into heightened neuronal activation during behavior. To address this, we quantified c-fos expression as a proxy for *in vivo* activity following exposure to the SA paradigm combined with 20 Hz optogenetic stimulation. Mice were perfused 70 minutes post-test to capture peak c-fos induction. Immunohistochemical analysis revealed c-fos expression in eYFP-labeled neurons across the B9, MRR and DRI (Fig. 5s). Quantification of the percentage of eYFP+ neurons co-expressing c-fos revealed a significant main effect of optogenetic stimulation across all three subregions in both sexes (Fig. 5t). In the B9 and DRI, optogenetic stimulation robustly increased the number of c-fos+ neurons in males and females to a similar extent (Fig. 5t). In contrast, in the MRR, a two-way ANOVA revealed both a significant main effect of treatment and a significant sex x treatment interaction, consistent with enhanced excitability of MRR 5-HT neurons in females (Fig. 5t). To quantify this differential increase in c-fos, we computed the stimulation-induced change from eYFP-controls in each sex, expressed as [(female ChETA – female eYFP) - (male ChETA – male eYFP)] (Fig. 5u). These findings indicate that while optogenetic activation of 5-HT^{vHP} neurons reliably drives neuronal activity across raphe subregions, MRR activation was greater in females, mirroring the observed sex-specific behavioral effects and increased intrinsic excitability of female MRR 5-HT^{vHP} neurons.

Collectively, these findings demonstrate that while 5-HT^{vHP} neurons are similarly distributed in male and female mice, female 5-HT^{vHP} neurons are more readily recruited, as revealed by c-fos mapping, and display subregion- and sex-specific differences in intrinsic properties. Whereas B9 and DRI neurons were largely similar between the sexes, MRR 5-HT^{vHP} are uniquely hyperexcitable, exhibiting more depolarized resting potentials, higher firing rates, reduced spike adaptation and spontaneous activity not observed in males or other subregions. Heightened intrinsic excitability of female MRR 5-HT^{vHP} neurons drives their disproportionate recruitment during behavior, providing a cellular mechanism for sex-specific vulnerability to anxiety.

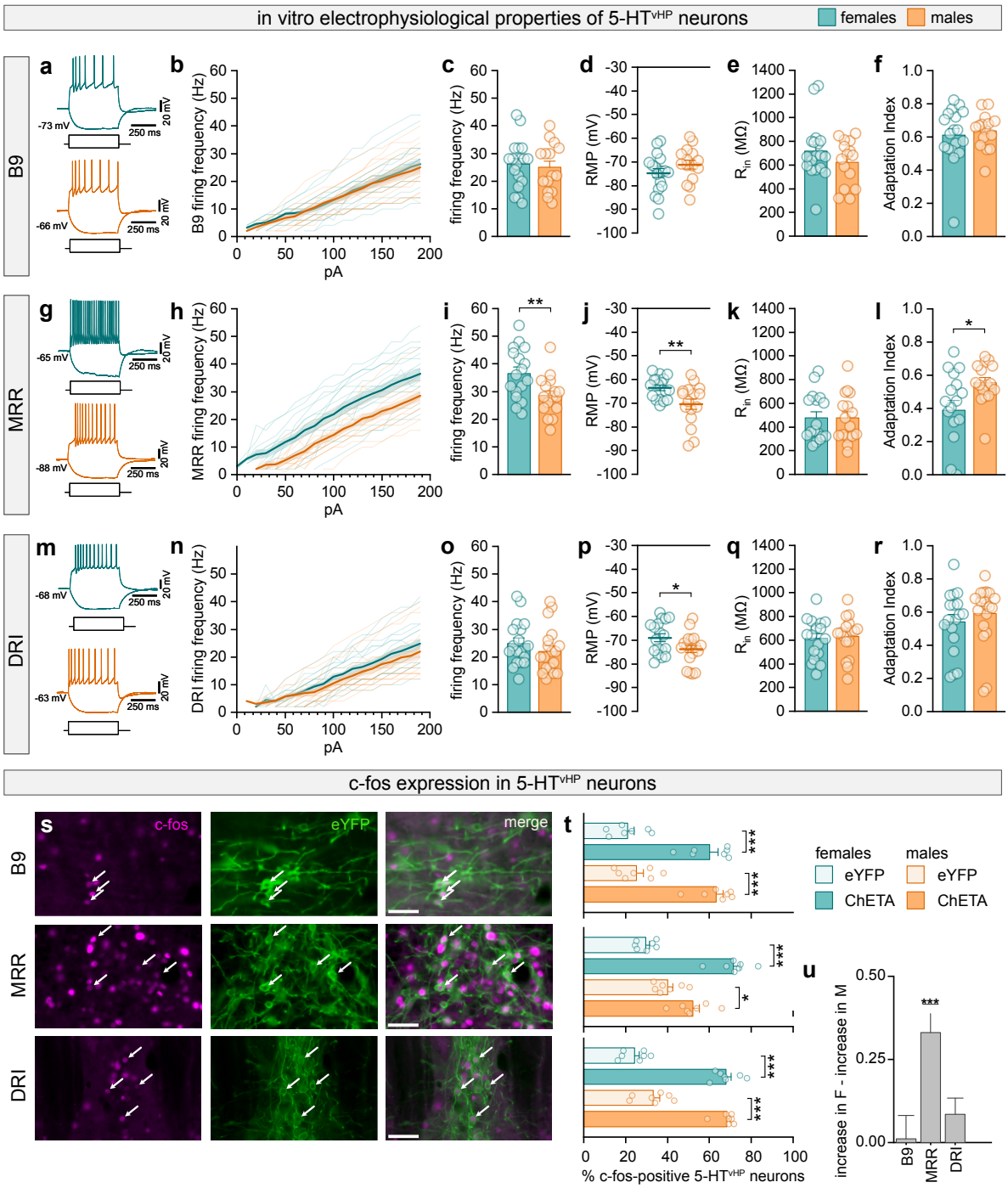

Figure 5: Female MRR 5-HT^{vHP} neurons exhibit increased intrinsic exitability. **a,** Examples of membrane potential responses to current steps (-50 pA for lower trace and + 190 pA for upper trace) as part of the electrophysiological characterization of eYFP+ neurons recorded from female (top) and male (bottom) animals for 5-HT^{vHP}, from the B9 nucleus. Number on the left indicates resting membrane potential. **b – f,** For B9 5-HT^{vHP} neurons, firing frequency responses as a function of current intensity stimulations (**b**), firing frequency at +190 pA (**c**), resting membrane potential (**d**), input resistance (**e**) and adaptation index (**f**) for females (teal, n = 18 cells from 9 mice) and males (orange, n = 15 cells from 10 mice). **g,** Same as **a,** for 5-HT^{vHP} neurons recorded from the MRR. **h – l,** Same as **b - f**, for eYFP+ neurons recorded from MRR. **i,** two sample t-test, P = 0.0089, **j,** two sample t-test, P = 0.0079, and **l,** two sample t-test, P = 0.0225, for females (teal, n = 17 cells from 6 mice and males (orange, n = 16 cells from 6 mice). **m**, Same as **a** and **g**, for eYFP+ neurons recorded from DRI. **n – r,** Same as for **b-f** and **h-l**, for eYFP+ neurons recorded from DRI. **p,** two sample t-test, P = 0.0207, for females (teal, n = 18 cells from 9 mice) and males (orange, n = 19 cells from 10 mice). **s,** Representative labeling of cFos (magenta) and retrograde eYFP (green)

expression in coronal sections of the B9, MRR and DRI. Arrows indicate examples of c-fos+/eYFP+ neurons. Scale bars = 50 µm. **t**, Percentage of eYFP+ neurons co-expressing c-fos in females (teal, eYFP: n = 7; ChETA: n = 7) and males (orange, eYFP: n = 7; ChETA: n = 7). Top: B9; two-way ANOVA with two-sample t-tests: females (ChETA vs control), $P < 0.0001$; males (ChETA vs control): $P < 0.0001$. Middle: MRR; two-way ANOVA with two-sample t-tests: females (ChETA vs control): $P < 0.0001$; males (ChETA vs control): $P = 0.0114$. Bottom: DRI; two-way ANOVA with two-sample t-tests, females (ChETA vs control), $P < 0.0001$; males (ChETA vs control: $P < 0.0001$. **u**, Stimulation induced change (stim – pre) for females relative to males in the number of c-fos+/eYFP+ neurons for each subregion. One sample t-test, MRR: P < 0.001. All data are shown as mean ± s.e.m. *: $P < 0.05$; **: $P < 0.01$; ***: $P < 0.001$; B9: B9 nucleus; MRR: median raphe region; DRI: dorsal raphe, interfascicular subregion; eYFP: enhanced yellow fluorescent protein. For detailed statistical information, see Extended Data Table 1.

Discussion

Mood and anxiety disorders disproportionately affect women, yet the neural substrates driving this sex bias remain poorly defined. Here, we identify serotonergic projections from the MRR to the vHP as a key neural substrate underlying sexually divergent anxiety responses. By integrating viral circuit tracing, retrograde fiber photometry, *in vivo* local field potential recordings, pathway specific optogenetics and patch-clamp electrophysiology, we demonstrate that this circuit displays robust sex differences that converge across multiple levels of analysis. Female MRR 5-HT^{vHP} neurons display increased intrinsic excitability, greater functional recruitment and a causal role in promoting anxiety-like responses. These findings offer a mechanistic framework for understanding how serotonergic circuits can differentially shape anxiety-related behaviors in females and contribute to sex-specific risk for mood disorders.

Consistent with previous work[14,61,89,90], we find that 5-HT^{vHP} neurons are distributed over multiple raphe subregions, notably the B9, MRR and DRI, with no differences in total number of 5-HT or 5-HT^{vHP} neurons between sexes. Our electrophysiological recordings revealed that MRR 5-HT^{vHP} neurons are intrinsically more excitable in females, exhibiting increased spontaneous activity, more depolarized resting membrane potentials and higher firing rates compared to males (Fig. 5). DRI 5-HT^{vHP} neurons in females also show depolarized membrane potentials, suggesting that intrinsic excitability may be an emergent property of subsets of serotonergic populations with shared developmental origins, connectivity and functions[12,91,92]. A few studies also report sex differences in the excitability of DR 5-HT neurons, but without specifying localization within DRI or projection targets[93,94]. In contrast, 5-HT^{vHP} neurons from the B9 group showed no sex differences in intrinsic properties. Together, these findings highlight striking electrophysiological heterogeneity in raphe-vHP circuits arising from B9, MRR and DRI. These raphe-vHP circuits might also show neurochemical diversity: the MRR and B9 contain 5-HT neuron populations of different embryonic origins that diverge into neurochemically distinct subtypes[95,96]. Notably, the MnR contains serotonergic neurons co-expressing the vesicular glutamate transporter VGLUT3, which project to the vHP[96–99], raising the possibility that a subset of the virus-transfected neurons in our study co-release glutamate and serotonin[53,100,101]. These diverse properties of raphe-vHP populations suggest that vHP functions are modulated by multiple specialized raphe circuits.

Our data link the intrinsic excitability of female MRR serotonergic neurons to heightened functional activation *in vivo*. Consistent with increased firing rates in MRR 5-HT^{vHP} neurons observed in slice electrophysiology (Fig. 5a-r), c-fos mapping revealed greater stimulation-induced recruitment of

MRR 5-HT^{vHP} neurons in female mice (Fig. 5s-u). In addition, *in vivo* calcium imaging revealed that MRR 5-HT^{vHP} neurons are dynamically, and sex-specifically, engaged during transitions into and out of the more aversive compartments of the EPM (Fig. 1). While 5-HT^{vHP} activity declined upon retreat into closed arms in both sexes, this decline was attenuated in females (Fig. 1i-j) and emerged only gradually over the session (Fig.1q-s). This delayed disengagement suggests a sex-specific persistence of neuronal activation, potentially reflecting slower updating of internal safety predictions under environmental novelty or threat. Strikingly, 5-HT^{vHP} neurons also displayed ramping activity in the seconds preceding exploration of the more aversive parts of the EPM, reminiscent of DR neuron ramping activity patterns observed during anticipation of reward or punishment[41,102–104]. Such progressive increases in DR 5-HT neuron activity over long timescales have recently been proposed to reflect a prospective coding for value[42], a framework that possibly extends to MRR 5-HT neurons. Notably, MRR and DR 5-HT neurons respond in opposite directions to rewarding stimuli[47], and also differ during locomotion: whereas DR neurons decrease their activity during locomotion bouts in the open field or avoidance tests[82], our findings confirm that in the same settings, MRR activity increases (Figure 1; Extended Data Fig. 1).

At the network level, targeted optogenetic activation of 5-HT^{vHP} neurons selectively disrupted dHP and vHP theta dynamics in female mice. Stimulation flattened the theta frequency-running speed relationship (Fig. 2), mirroring the pattern typically seen during novelty exposure and consistent with a failure to habituate to the environment[75,77,79]. In contrast, control animals and male ChETA mice exhibited the expected progressive slope increase over time, reflecting familiarization. These findings extend previous results showing serotonergic modulation of hippocampal theta[105–108] by demonstrating a sex-dependent effect. Given that, during anxiety states, theta synchrony facilitates long-range communication between the hippocampus and other regions, such as the PFC[29,32,109], serotonergic modulation of vHP theta could maintain persistent vigilance. This interpretation is supported by our anatomical mapping (Extended Data Fig. 7), which revealed collateral projections from 5-HT^{vHP} neurons to the PFC, raising the possibility that their activation coordinates distributed circuits implicated in anxiety regulation.

Behaviorally, optogenetic activation of 5-HT^{vHP} neurons increased anxiety-like behavior selectively in females. In ethologically relevant tests, including the EPM and SA, female ChETA mice exhibited increased avoidance of anxiogenic zones (Fig. 3c-f), reduced risk-assessment behaviors such as head-dipping and stretch-attend postures (Fig. 3g-j), and increased stress-related grooming (Fig. 4). Notably, grooming was selectively elevated in anxiogenic environments but unaffected in the open field (Fig. 4h-j), highlighting the context dependence of this circuit's behavioral impact, in line with past work[46]. The observation that grooming episodes were associated with rapid decreases in calcium signal in both sexes (Fig. 4a-g) supports the view of grooming as an adaptive displacement behavior[87,110,111], which transiently suppresses serotonergic tone.

Importantly, the behavioral effects of 5-HT^{vHP} neuron activation occurred in the near absence of locomotor changes (Extended Data Fig. 6b-j), supporting a specific role in anxiety modulation behavior rather than general arousal. While broad activation of the MnR has previously been shown to

increase anxiety-like behavior[9,44,80], our data refine this understanding by demonstrating that selective stimulation of the vHP projection pathway is sufficient to amplify anxiety-related behaviors in females. Although our c-fos data show robust activation of 5-HT neurons in both sexes (Fig. 5), stimulation did not alter anxiety-related behaviors in males. This dissociation suggests that, in males, the vHP-projecting serotonergic pathway may primarily contribute to behavioral domains not captured by the behavioral paradigms used here. The MnR provides dense serotonergic innervation to a wide array of forebrain regions[61], and individual 5-HT neurons collateralize extensively[89,90]. Although 5-HT^{vHP} neurons also collateralize to other forebrain regions, including the dHP and lateral septum, which could contribute to their behavioral effects, we found no sex differences in collateral density or distribution (Extended Data Fig. 7), suggesting that differential downstream targeting is unlikely to account for the sex-specific responses. The postsynaptic mechanisms mediating serotonergic modulation of vHP outputs remain unknown. Given that virtually all 5-HT receptor subtypes are expressed in the vHP[112], serotonergic input to this region could act on multiple parallel output pathways, including to anxiety-related regions such as prefrontal cortex, lateral hypothalamic area or lateral septum[26,113–116]. The details of 5-HT modulation of vHP long-range principal cells or interneurons, and their impact on sex specific anxiety responses await clarification.

Overall, our findings advance an emerging body of work delineating the roles of topographically organized serotonergic circuits in the modulation of emotion-related behaviors[19,47,117,118]. Our study directly links hyperexcitability of the female MRR 5-HT^{vHP} pathway to enhanced anxiety-like responses. These findings align with the higher prevalence of anxiety and mood disorders in women[119–121], and suggests that sex-specific serotonergic circuit function may constitute a core vulnerability factor across affective disorders. By delineating a projection-specific serotonergic pathway that differentially modulates anxiety-related behaviors in females, our work highlights the potential for sex-informed, circuit-targeted interventions in mood and anxiety disorders.

Acknowledgements

We thank Dr. Elke Küster-Schöck from the Centre Hospitalier Universitaire Sainte-Justine Imaging center for microscopy guidance, and Denise Carrier, Véronique Pelletier and the animal facility team for help with colony maintenance. We thank all members of the Amilhon lab for their valuable comments on the manuscript, and undergraduate students Clémence Brin, Camille Pons, Charlène Manti, Morgane Roger for their help with various aspects of the study.

Funding

S.v.d.V. was supported by a CIHR postdoctoral fellowship and a Fonds de Recherche du Quebec - Santé (FRQS) postdoctoral fellowship. J.F.H. was supported by a Canada doctoral graduate scholarship from the Natural Sciences and Engineering Research Council of Canada (NSERC) and by a complement scholarship from the Fonds de recherche du Québec (FRQ). A.-S.S. was supported by

a recruitment grant from the Department of Neuroscience at the Université de Montréal. This work was funded by the Canadian Institutes for Health Research (CIHR) #173244, NARSAD Young Investigator Grant #25287, the Réseau Québécois sur le Suicide et les troubles de l'Humeur Associés, the Brain Canada Future Leaders program, the Fonds de Recherche du Québec – Santé and the Canadian Foundation for Innovation to B.A.

The funders had no role in study design, data collection or analysis.

Contributions

S.v.d.V. performed LFP experiments. F.H. performed fiber photometry and double-projection experiments. L.P. performed patch-clamp electrophysiology experiments. A.-S.S. and F.P. performed optogenetic experiments. J.F.H. and A.-S.S. collected collateral dataset. A.-S.S., F.P. and F.H. performed c-fos experiments. S.v.d.V. and G.D. developed analysis pipelines and code. G.D. provided technical support for all experiments and statistical analysis. All authors analyzed data, performed statistical analysis and provided material for the manuscript. S.v.d.V. and B.A. prepared figures and wrote the manuscript with contribution and input from all authors. B.A. conceived and supervised all aspects of the project, and secured funding. L.P. and F.H. contributed equally to this work.

Ethics declarations

Competing interests: The authors declare no competing interests.

Materials and methods

Animals

Male or female SERT-Cre (B6.FVB(Cg)-Tg(Slc6a4-cre)ET33Gsat/Mmucd line, MMR ,#031028-UCD;) transgenic mice were bred with female or male C57BL/6J mice (Jackson Laboratory, #000664) to generate experimental animals. All mice used in this study were between 60-90 days old at the time of experiments. Animals were group-housed on a 12-hour light/dark cycle at 24°C and 40% humidity with ad libitum access to food and water. All procedures involving animals were approved by the Comité Institutionnel des Bonnes Pratiques Animales en Recherche (CIBPAR) of the Centre de Recherche Azrieli du CHU Sainte-Justine (protocol 2023-5039), in accordance with the standards of the Canadian Council on Animal Care.

Stereotaxic surgeries

Animals were anesthetized with isoflurane (5% induction, 0.5-1.5% maintenance) and placed in a stereotaxic frame (David Kopf instruments). Carprofen (2 mg/kg) was administered subcutaneously before surgery. Body temperature was maintained at 37°C with a heating pad (Stoelting) and eyes were

hydrated with ocular gel (Optixcare, Aventix). Craniotomies were performed using a mountable drill (Stoelting). Viral injections were performed using a glass pipette backfilled with mineral oil connected to a Nanoject III (Drummond Scientific) at a flow rate of 1 nL/second. To target 5-HT^{vHP} neurons, a retrogradely transported adeno-associated virus (AAV) of serotype 2/9 was bilaterally infused in the vHP. Each hippocampus received 400 nL of viral solution injected at two sites (stereotaxic coordinates: [AP] -3.52, [ML] ±3.25, [DV] -4.17 and -3.47). All stereotaxic coordinates are taken from bregma (in mm).

For electrode and optic fiber implantation surgeries, the skull was exposed and carefully cleaned with ethanol before craniotomies were drilled. Electrodes and/or optic fiber were then slowly lowered into position and maintained in place using a combination of C&B-Metabond and dental acrylic (Parkell) and 2-3 stainless-steel anchor screws (Antrin Miniature Specialties Inc). Electrodes and optic fiber stereotaxic coordinates are described in the corresponding sections below. Following surgery, mice were monitored for at least 3 days and allowed to recover for at least one week before subsequent procedures or behavioral testing.

Fiber photometry recordings

SERT-Cre mice received bilateral injections of AAV2/9-Syn-Flex-GCaMP6s-WPRE-SV40 (CS1028, University of Pennsylvania Vector Core) targeting the vHP using the methodology described above, resulting in retrograde expression of the calcium indicator GCaMP6s in 5-HT^{vHP} neurons. Four weeks later, animals were implanted with a 200 µm low-autofluorescence optic fiber cannula (Neurophotometrics) targeting GCaMP6s transfected neurons in the MRR ([AP] – 4.20 to – 5.30 with a 10° rostro-caudal angle, [ML] 0.00, [DV] – 3.5 to – 4.45).

Following implantation and recovery, mice were habituated for at least one week. They were handled daily, connected to sham patchcords in individual home cages containing familiar bedding and nesting material, and then returned to their littermates before the dark cycle. Behavioral testing was conducted on separate days in either a in a 40 x 40 cm light grey square open field (40 x 40 cm light grey square) or an EPM consisting of two closed arms (30 x 5 x 19.8 cm) and two open arms (30 x 5 x 0.9 cm), and a 5 x 5 cm center zone. On each testing day, mice were first habituated for 1 hour in individual cages in the experimental room. After habituation, mice were connected to the patchcord and returned to the cage for 20 minutes during which photometry recording was initiated. Animals were then placed in the behavioral apparatus for 20 minutes of free exploration.

Excitation light (470 nm and 415 nm) was alternately pulsed at 10 Hz at ~80 µW (measured at the fiber tip) using an FP3002 photometry console (Neurophotometrics). Arenas were cleaned with water and 70% ethanol between animals. Room illumination was maintained at 70 ± 10 lux. Fluorescence was recorded sequentially for both the 470 nm calcium-dependent signal and the 415 nm isosbestic control. Injection sites, viral expression, and fiber placements were verified post hoc by histology, as described below.

Bleaching and movement artifacts were corrected using the method previously described[122]. Briefly, we used the coefficient obtained from a linear fit (obtained from iteratively reweighted least

squares regression) of the 415 nm signal to the 470 nm signal, to scale the 415 nm signal. The scaled 415 nm signal was subtracted from the 470 nm signal to obtain ΔF, and ΔF was divided by the scaled 415 nm signal to yield ΔF/F. Signals were z-scored across the recording session and low-pass filtered at 3 Hz prior to further analysis. Peri-event plots were generated for each mouse by averaging z-scored ΔF/F around behavioral events and subtracting the baseline (average signal 1-2 s prior to the event). Within-mouse averages were then averaged across animals to obtain group means.

Mouse body parts were tracked using SLEAP[123], and the center of the body was used for all subsequent analyses. Animal positions were filtered to reduce jitter: the animal position at a specific frame was updated only if the raw animal position for that frame was located further than ½ of the mouse length away from the previous position. Movement initiation was defined as the first frame where velocity exceeded 1 cm/s, provided the mouse moved < 2 cm in the preceding 1 s period and > 10 cm in the subsequent second.

For the transitions between closed and open arms in the EPM (Fig. 1d-g), closed→open transitions were defined as the mouse spending at least 10 s in a closed arm before entering center/open arms for ≥ 2 s. Closed→closed transitions were defined as transitions between closed arms with ≤ 1 s spent in the center. Changes in fluorescence were aligned to the timepoint at which center-of-body crossed the closed arm-center boundary. For time-locked analysis of closed-arm entries and exits (Fig. 1h-s), arm entries were included in the analysis if the mouse spent ≥ 2 s in the center/open arm before entering the closed arm, and ≥ 2 s in the closed arm after entry. Exit transitions were defined similarly, requiring at least 2 s in the closed arm before transition and at least 2 s in the center or open arm after exit. Grooming onset and offset were manually scored frame-by-frame using custom Matlab code.

Local field potential recordings

SERT-Cre mice received bilateral vHP injection of either AAV2/9-EF1a-DIO-hChR2(E123T/T159C)-eYFP (#35509-AAV9, Addgene), to cause CRE-dependent expression of the excitatory opsin ChETA in vHP projecting 5-HT neurons, or AA2/9-EF1a-DIO-eYFP (#27056-AAV9, Addgene) for control mice, using the methodology described above. Three weeks after virus injection, animals were implanted with a 200 µm optic fiber (#FG200UEA, Thorlabs) above the MRR ([AP] -4.35, [ML] -0.55 at 7° angle, [DV] -3.23), and custom recording electrodes in the hippocampus. For local field potential (LFP) recordings, custom bipolar electrodes were constructed using 50 µm PFA coated tungsten wire (#585088, A-M Systems) and targeted to the ventral ([AP] -3.65, [ML] 3.50, [DV] -3.00) and dorsal hippocampus ([AP]: -1.58, [ML] 1.40, [DV] -1.50). A ground screw was placed over the cerebellum and an EMG electrode was implanted in the trapezius muscle. All electrode and fiber placements were confirmed by histology, as described below. LFP were recorded and digitized at 20 KHz using an Open Ephys system[124], while mice explored a novel, circular open field (39 cm diameter).

Videos were processed with DeepLabCut[125,126] (version 2.3rc3) to extract body positions, using the body center as the animal's position. LFP recordings were down sampled to 1 kHz and aligned with the behavioral tracking data. LFPs were band-pass filtered (5-10 Hz) and subjected to a Hilbert

transform to obtain the analytic signal. The power of the signal was taken as the magnitude of the analytic signal squared. The instantaneous phase of the analytic signal was extracted and unwrapped to provide an estimation of instantaneous theta frequency. Periods with power >6 SD were considered movement artefacts and were removed from analysis along with the flacking 250ms of data on each side.

Animal positions were filtered to reduce jitter as described in the fiberphotometry section. Running speed was computed from the filtered positions by dividing Δd/Δt where d is the distance and t is time. Finally, to characterize the relationship between theta frequency and running speed, the median of the instantaneous frequency was taken over a time window of approximately 33.3ms to yield a frequency estimate corresponding to each frame of the video (sampled at 30 Hz). A first order polynomial was fitted to theta frequency and animal speed between 1 and 30 cm/s to extract the slope and intercept of the speed – theta frequency relationship.

Optogenetic manipulations and behavior

5-HT^{vHP} neurons of SERT-Cre mice were transfected with either the excitatory opsin ChETA or eYFP, and an optic fiber was implanted as described above. Mice were allowed a 2-week recovery period post-implantation, followed by 5 days of handling (~10min/day) to minimize stress related to the experimenter, the behavior room or the fiber optic connection on the day of the experiment. On testing days, mice were transferred to the experimental room ≥ 45 min before behavioral assays and placed in individual cages containing familiar bedding and nesting material. All experiments were conducted between 9 AM and 2 PM to reduce circadian variability.

Behavioral testing occurred in the following order with 48 h intervals between tests: open field, EPM, and SA. Arenas were cleaned with 70% ethanol between mice to reduce olfactory cues, and light sensitivity was maintained at 70 ± 5 lux at the center of each apparatus. Mice were allowed to freely explore the maze for 12 min, with optogenetic stimulation delivered during minutes 4-8. Stimulation consisted of blue light (450 nm) pulses at 20 Hz (10 ms pulse width) at ~15 mW measured at the fiber tip. Viral expression and fiber placement were confirmed post hoc (see Histology).

Mouse body parts were extracted from each video using SLEAP[123], using the center of the body as the animal's position. From this raw animal position, the time spent and the number of entries in each zone of the different mazes could be computed. Entries into a zone were recorded if the raw animal position was within the zone for at least 1s. To compute the distance traveled and animal velocity, we filtered the raw animal position as described in the previous section. From this filtered position, the distance traveled was computed as the sum of the frame-to-frame displacement, and velocity was obtained by multiplying frame-by-frame displacements by the video sampling frequency. The time immobile was taken as the total time where the animal was not locomoting and the mean velocity while moving was calculated from all periods of locomotion.

For the successive alleys an anxiety index was calculated as:

$$Anxiety\ Index\ = \frac{1\times T_{Z1} + \frac{2}{3}\times T_{Z2} + \frac{1}{3}\times T_{Z3} + 0\ \times T_{Z4}}{T_{total}}$$

Where T_{z1} -T_{z4} are time spent in zones 1-4 and T_{total} is total test duration. Values near 1 indicate that mice spent most of their time in less aversive zones (zone 1). Values near 0.5 reflect uniform exploration across zones. These scores can also be interpreted as the normalized mean position of the mouse along the alleys from zone 1 to zone 4. Grooming, rearing, stretching and head-dipping behaviors were manually scored by the same experimenter blind to treatment (eYFP or ChETA).

Histology

For all immunohistochemistry experiments, mice were deeply anesthetized with an intraperitoneal injection of ketamine/xylazine/acepromazine (80/12.5/2.5 mg/kg, respectively). Animals were transcardially perfused with 45 mL of 4% paraformaldehyde (PFA) in phosphate-buffered saline (PBS), and brains were extracted and postfixed in PFA at 4°C for 24-48 h. For cryosectioning, brains were cryoprotected using 15% sucrose in PBS for 24 h, embedded in Tissue-Plus™ O.C.T. Compound (#23-730-571, Fisher Scientific), and frozen in isopentane. Standard immunohistochemistry was performed using antibody solutions prepared in PBS with 0.45% gelatin and 0.25% triton. Image processing and analysis were performed using FIJI software (ImageJ, version 2.14.0). When necessary, Tph2 immunolabelling was used to delineate the raphe nuclei.

Histological validation of viral expression, electrode and fiber placement

For anatomical validation of viral expression and optical fiber implantation sites, frozen coronal sections (25 µm) were prepared and cut on a cryostat (Leica Biosystems CM3050 S), and stained for eYFP or GCaMP6s and Tph2 as described above, using the following primary and secondary antibodies: anti-Tph2 in guinea pig (1:1000; #TPH2-GP-Af900, Frontier Institute), anti-GFP in chicken (1:2000; #A10262, Invitrogen), anti-chicken A488 in donkey (1:2000; #703-545-155, Jackson ImmunoResearch) and anti-guinea pig A647 in goat (1:2000; #A21450, ThermoFisher). Sections were mounted on slides using Fluoromount-G containing DAPI (ThermoFisher). Images were acquired using a Leica DMi8 wide-field inverted microscope with 10X and 20X objectives, equipped with a Leica DFC9000 camera, and LAS X software (Leica). For electrophysiology experiments, fixed (non-frozen) brains were sectioned at 40 µm using a vibratome (Leica VT1200) and collected sequentially. One-quarter of the sections were stained for eYFP and Tph2, as described above, to assess viral expression and optical fiber placement, while the remaining three quarters were directly mounted to assess HP electrode placement. These sections were imaged using the Zeiss AxioScan.Z1 with 10X objective and ZEN Microscopy Software (Zeiss).

Collaterals

To assess the proportion of 5-HT neurons projecting to both the dHP and vHP (Extended Data Fig. 4), adult SERT-Cre males (n = 3) and females (n = 4) were injected as described above with AAV2/9-EF1a-DIO-hChR2(E123T/T159C)-eYFP (#35509-AAV9, Addgene) in the left vHP (2 injections of 400 nL of virus). Five weeks later, neurons projecting to the left dHP were retrogradely labeled with CTB-A647, using 100 µg of CTB-A647 previously suspended in 20 µl of PBS1x at 4 °C and short-term stored at 4 °C. dHP injections were performed at: [AP] -1.90 and -2.40, [ML] -1.35 and -2.00, [DV] -1.55 and -1.65. Mice were sacrificed 10 days post CTB injection. Coronal sections were cut (35 µm) on a

vibratome (Leica VT1200) and labeled for eYFP and Tph2 using the following primary and secondary antibodies: anti-GFP in goat (1:5000; #NB100-1770, Novus Biologicals), anti-Tph2 in rabbit (1:2000; #NB100-74555, Novus Biological), anti-goat-A488 in donkey (1:2000; #A11055, Life Technologies) and anti-rabbit-A555 in donkey (1:2000; #A31572, Life Technologies). The distribution of HP-projecting 5-HT neurons was quantified on sections collected at 105 µm intervals along the rostro-caudal axis of the raphe nuclei (B5-B9).

For qualitative assessment of 5-HT^{vHP} collaterals (Extended Data Fig. 7), a separate group of SERT-Cre males (n = 4) and females (n = 4) was used. 5-HT^{vHP} neurons were transfected using bilateral injections as described above. Free-floating coronal and horizontal slices (25 µm) were cut on a cryostat (Leica Biosystems CM3050 S) and labeled for eYFP and 5-HT using the following primary and secondary antibodies: anti-GFP in chicken (1:2000; #A10262, Invitrogen), anti-5-HT in goat (1:2000; #ab66047, Abcam), anti-chicken-A488 in donkey (1:2000; #703-545-155, Jackson ImmunoResearch) and anti-goat-A555 in donkey (1:2000; #A21432, Thermo Fisher Scientific). All regions with collaterals were identified using anatomical landmarks and a mouse brain atlas[127] as reference. All images were acquired using a Leica DMi8 wide-field inverted microscope as described above.

C-fos assessment of neural activity

C-fos expression was assessed in mice expressing ChETA or eYFP in 5-HT^{vHP} neurons. Mice were sacrificed 70 minutes after completing 12 minutes in the SA paradigm with optogenetic stimulation performed as described above. Fixed, non-frozen brains were cut into 40 µm sections using a vibratome (Leica VT1200) and triple-labeled for c-fos, eYFP and Tph2 using the same protocol, with the addition of anti-c-fos in rabbit (1:2000; #2250, Cell Signalling) and anti-rabbit –A555 in donkey (1:2000; #A31572, Life Technologies). The distribution of 5-HT+/c-fos+/eYFP+ neurons was quantified on sections collected at 120 µm intervals along the rostro-caudal axis of the raphe nuclei.

Patch-clamp

Mice were deeply anesthetized with isoflurane and brains were prepared for sectioning on a vibratome using a modified protocol from Ting and colleagues[128]. Each mouse was transcardially perfused with an NMDG-based solution (in mM: 93 NMDG, 93 HCl, 2.5 KCl, 1.2 NaH2PO4, 30 NaHCO3, 20 HEPES, 25 glucose, 5 sodium ascorbate, 2 thiourea, 3 sodium pyruvate, 10 MgSO4, and 0.5 CaCl2 at pH 7.4, oxygenated with carbogen). Coronal sections (300 µm) were cut using a vibratome (Leica VT1200) and incubated at 32°C for 10 to 12 minutes in the same NMDG solution. Slices were then transferred to artificial cerebrospinal fluid (aCSF) at room temperature (in mM: 124 NaCl, 24 NaHCO3, 2.5 KCl, 1.2 NaH2PO4, 5 HEPES, 12.5 glucose, 2 MgSO4, and 2 CaCl2, pH 7.4, oxygenated with carbogen). During recordings, slices were continuously perfused with aCSF at 28°C at 3 mL/min.

5-HT^{vHP} neurons were visually identified via eYFP fluorescence. Whole-seal recordings were obtained using an intrapipette solution (in mM: 126 K-gluconate, 4 KCl, 10 HEPES, 4 Mg2ATP, 0.3 Na2GTP, and 10 PO-Creatine, adjusted to pH 7.25 with KOH; 272 mOsm). Pipette had a resistance between 4 to 8 MΩ. Recordings were performed using an Axon Multiclamp 700B amplifier (Molecular Devices). After achieving whole-cell configuration, resting membrane potential was recorded for 4 min

prior to additional protocols. In current-clamp, 500 ms hyperpolarizing steps were applied to assess hyperpolarization-activated current, passive membrane conductance and input resistance. 500 ms depolarizing current steps were applied to assess firing frequency, rheobase and action potential features. The adaptation index was calculated using the last depolarizing current step as:

$$AI = 1 - \left(\frac{ISI_i}{ISI_l}\right)$$

where ISI_i and ISI_l are the initial and last interspike interval (ISI), respectively. All membrane potentials were corrected offline for a liquid junction potential (LJP) of -15.8mV.

Statistics

All data are presented as mean ± standard error of the mean (s.e.m.), and the corresponding statistical tests are described in the figure legends and in Extended Data Table 1, and Extended Data Table 2. Origin 2024 (OriginLab) was used for all basic statistical analysis, except for behavioral experiments described in Figure 4 and Figure 5, which were analyzed with R (version 4.4.1 in RStudio 2025.05.0).

Behavioral experiments were conducted on two independent cohorts, and therefore analyzed with three-way ANOVA with sex, treatment and cohort as factors. The ANOVA model included all main effects (sex, treatment and cohort) and interactions (sex * treatment, sex * cohort, treatment * cohort and sex * treatment * cohort). Post hoc tests were performed for planned comparisons (female-eYFP vs. male-eYFP, female-eYFP vs. female-ChR2, male-eYFP vs. male-ChR2 and female-ChR2 vs. male-ChR2) using Holm's correction for multiple testing. Statistical tests were performed in R using the *aov* function (stats package) for the three-way ANOVA and the *emmeans* function (*emmeans* package) for post hoc comparisons. Homogeneity of variance was tested using Levene's test *(leveneTest* function, *car* package) using median[129]. For clarity, only the plots of the marginal means are shown in the main text, while the full group breakdown is shown in Extended Data Table 1. A threshold of $P < 0.05$ was considered statistically significant. Figures use the following significance notation: *, $P < 0.05$; **, $P < 0.01$; ***, $P < 0.001$.

References

1. Bangasser, D. A. & Cuarenta, A. Sex differences in anxiety and depression: circuits and mechanisms. *Nat Rev Neurosci* **22**, 674–684 (2021).
2. McLean, C. P., Asnaani, A., Litz, B. T. & Hofmann, S. G. Gender differences in anxiety disorders: Prevalence, course of illness, comorbidity and burden of illness. *Journal of Psychiatric Research* **45**, 1027–1035 (2011).
3. Kaluve, A. M., Le, J. T. & Graham, B. M. Female rodents are not more variable than male rodents: A meta-analysis of preclinical studies of fear and anxiety. *Neuroscience & Biobehavioral Reviews* **143**, 104962 (2022).

4. Graeff, F. G. & Zangrossi, H. The dual role of serotonin in defense and the mode of action of antidepressants on generalized anxiety and panic disorders. *Cent Nerv Syst Agents Med Chem* **10**, 207–217 (2010).
5. Ren, J. *et al.* Anatomically defined and functionally distinct dorsal raphe serotonin sub-systems. *Cell* **175**, 472-487.e20 (2018).
6. Marcinkiewcz, C. A. *et al.* Serotonin engages an anxiety and fear-promoting circuit in the extended amygdala. *Nature* **537**, 97–101 (2016).
7. Urban, D. J. *et al.* Elucidation of the behavioral program and neuronal network encoded by dorsal raphe serotonergic neurons. *Neuropsychopharmacology* **41**, 1404–1415 (2016).
8. Teissier, A. *et al.* Activity of raphé serotonergic neurons controls emotional behaviors. *Cell Reports* **13**, 1965–1976 (2015).
9. Ohmura, Y. *et al.* Different roles of distinct serotonergic pathways in anxiety-like behavior, antidepressant-like, and anti-impulsive effects. *Neuropharmacology* **167**, 107703 (2020).
10. Okaty, B. W., Commons, K. G. & Dymecki, S. M. Embracing diversity in the 5-HT neuronal system. *Nat Rev Neurosci* **20**, 397–424 (2019).
11. Gaspar, P. & Lillesaar, C. Probing the diversity of serotonin neurons. *Philosophical Transactions of the Royal Society B: Biological Sciences* **367**, 2382–2394 (2012).
12. Hale, M. W. & Lowry, C. A. Functional topography of midbrain and pontine serotonergic systems: implications for synaptic regulation of serotonergic circuits. *Psychopharmacology* **213**, 243–264 (2011).
13. Awasthi, J. R., Tamada, K., Overton, E. T. N. & Takumi, T. Comprehensive topographical map of the serotonergic fibers in the male mouse brain. *Journal of Comparative Neurology* **529**, 1391–1429 (2021).
14. Muzerelle, A., Scotto-Lomassese, S., Bernard, J. F., Soiza-Reilly, M. & Gaspar, P. Conditional anterograde tracing reveals distinct targeting of individual serotonin cell groups (B5–B9) to the forebrain and brainstem. *Brain Struct Funct* **221**, 535–561 (2016).
15. Gagnon, D. & Parent, M. Distribution of VGLUT3 in highly collateralized axons from the rat dorsal raphe nucleus as revealed by single-neuron reconstructions. *PLoS One* **9**, e87709 (2014).
16. Ren, J. *et al.* Single-cell transcriptomes and whole-brain projections of serotonin neurons in the mouse dorsal and median raphe nuclei. *eLife* **8**, e49424 (2019).
17. Sharp, T. & Barnes, N. M. Central 5-HT receptors and their function; present and future. *Neuropharmacology* **177**, 108155 (2020).
18. Vilaró, M. T., Cortés, R., Mengod, G. & Hoyer, D. Distribution of 5-HT receptors in the central nervous system: an update. in *Handbook of the Behavioral Neurobiology of Serotonin* (eds. Müller, C. P. & Cunnigham, K. A.) vol. 31 (Academic Press, 2020).
19. Yu, X.-D. *et al.* Distinct serotonergic pathways to the amygdala underlie separate behavioral features of anxiety. *Nat Neurosci* **25**, 1651–1663 (2022).

20. Béïque, J.-C. *et al.* Serotonergic regulation of membrane potential in developing rat prefrontal cortex: coordinated expression of 5-hydroxytryptamine (5-HT)1A, 5-HT2A, and 5-HT7 receptors. *J Neurosci* **24**, 4807–4817 (2004).
21. Teixeira, C. M. *et al.* Hippocampal 5-HT input regulates memory formation and schaffer collateral excitation. *Neuron* **98**, 992-1004.e4 (2018).
22. Kjelstrup, K. G. *et al.* Reduced fear expression after lesions of the ventral hippocampus. *Proc. Natl. Acad. Sci. U.S.A.* **99**, 10825–10830 (2002).
23. Gray, J. A. & McNaughton, N. *The Neuropsychology of Anxiety: An Enquiry into the Function of the Septo-Hippocampal System*. (OUP Oxford, 2003).
24. Strange, B. A., Witter, M. P., Lein, E. S. & Moser, E. I. Functional organization of the hippocampal longitudinal axis. *Nat Rev Neurosci* **15**, 655–669 (2014).
25. Bannerman, D. M. *et al.* Regional dissociations within the hippocampus--memory and anxiety. *Neurosci Biobehav Rev* **28**, 273–283 (2004).
26. Jimenez, J. C. *et al.* Anxiety cells in a hippocampal-hypothalamic circuit. *Neuron* **97**, 670-683.e6 (2018).
27. Parfitt, G. M. *et al.* Bidirectional control of anxiety-related behaviors in mice: role of inputs arising from the ventral hippocampus to the lateral septum and medial prefrontal cortex. *Neuropsychopharmacology* **42**, 1715–1728 (2017).
28. Ciocchi, S., Passecker, J., Malagon-Vina, H., Mikus, N. & Klausberger, T. Selective information routing by ventral hippocampal CA1 projection neurons. *Science* **348**, 560–563 (2015).
29. Adhikari, A., Topiwala, M. A. & Gordon, J. A. Synchronized activity between the ventral hippocampus and the medial prefrontal cortex during anxiety. *Neuron* **65**, 257–269 (2010).
30. Adhikari, A., Topiwala, M. A. & Gordon, J. A. Single units in the medial prefrontal cortex with anxiety-related firing patterns are preferentially influenced by ventral hippocampal activity. *Neuron* **71**, 898–910 (2011).
31. Li, K., Koukoutselos, K., Sakaguchi, M. & Ciocchi, S. Distinct ventral hippocampal inhibitory microcircuits regulating anxiety and fear behaviors. *Nat Commun* **15**, 8228 (2024).
32. Padilla-Coreano, N. *et al.* Direct ventral hippocampal-prefrontal input is required for anxiety-related neural activity and behavior. *Neuron* **89**, 857–866 (2016).
33. Royer, S., Sirota, A., Patel, J. & Buzsáki, G. Distinct representations and theta dynamics in dorsal and ventral hippocampus. *J Neurosci* **30**, 1777–1787 (2010).
34. Cerquetella, C., Gontier, C., Forro, T., Pfister, J.-P. & Ciocchi, S. Scaling of ventral hippocampal activity during anxiety. *J Neurosci* **45**, e1128242025 (2025).
35. Sánchez-Bellot, C., AlSubaie, R., Mishchanchuk, K., Wee, R. W. S. & MacAskill, A. F. Two opposing hippocampus to prefrontal cortex pathways for the control of approach and avoidance behaviour. *Nat Commun* **13**, 339 (2022).
36. Yeates, D. C. M. *et al.* Parallel ventral hippocampus-lateral septum pathways differentially regulate approach-avoidance conflict. *Nat Commun* **13**, 3349 (2022).

37. Badarnee, M., Wen, Z., Nassar, N. & Milad, M. R. Gray matter associations with extinction-induced neural activation in patients with anxiety disorders. *Journal of Psychiatric Research* **162**, 180–186 (2023).
38. Bach, D. R. *et al.* Human hippocampus arbitrates approach-avoidance conflict. *Curr Biol* **24**, 541–547 (2014).
39. Ito, R. & Lee, A. C. H. The role of the hippocampus in approach-avoidance conflict decision-making: Evidence from rodent and human studies. *Behavioural Brain Research* **313**, 345–357 (2016).
40. Paquelet, G. E. *et al.* Single-cell activity and network properties of dorsal raphe nucleus serotonin neurons during emotionally salient behaviors. *Neuron* **110**, 2664-2679.e8 (2022).
41. Sengupta, A. & Holmes, A. A discrete dorsal raphe to basal amygdala 5-HT circuit calibrates aversive memory. *Neuron* **103**, 489-505.e7 (2019).
42. Harkin, E. F., Grossman, C. D., Cohen, J. Y., Béïque, J.-C. & Naud, R. A prospective code for value in the serotonin system. *Nature* **641**, 952–959 (2025).
43. Dayan, P. & Huys, Q. J. M. Serotonin in affective control. *Annual Review of Neuroscience* **32**, 95–126 (2009).
44. Andrade, T. G. & Graeff, F. G. Effect of electrolytic and neurotoxic lesions of the median raphe nucleus on anxiety and stress. *Pharmacol Biochem Behav* **70**, 1–14 (2001).
45. De Almeida, R. M., Giovenardi, M., Charchat, H. & Lucion, A. B. 8-OH-DPAT in the median raphe nucleus decreases while in the medial septal area it may increase anxiety in female rats. *Neurosci Biobehav Rev* **23**, 259–264 (1998).
46. Ahmadlou, M. *et al.* A subcortical switchboard for perseverative, exploratory and disengaged states. *Nature* **641**, 151–161 (2025).
47. Kawai, H. *et al.* Median raphe serotonergic neurons projecting to the interpeduncular nucleus control preference and aversion. *Nat Commun* **13**, 7708 (2022).
48. Maddaloni, G., Chang, Y. J., Senft, R. A. & Dymecki, S. M. Adaptation to photoperiod via dynamic neurotransmitter segregation. *Nature* **632**, 147–156 (2024).
49. Huang, X. *et al.* A circuit from lateral hypothalamic to dorsal hippocampal dentate gyrus modulates behavioral despair in mice. *Cerebral Cortex* **34**, bhae399 (2024).
50. Yoshida, K., Drew, M. R., Mimura, M. & Tanaka, K. F. Serotonin-mediated inhibition of ventral hippocampus is required for sustained goal-directed behavior. *Nat Neurosci* **22**, 770–777 (2019).
51. Abela, A. R. *et al.* Median raphe serotonin neurons promote anxiety-like behavior via inputs to the dorsal hippocampus. *Neuropharmacology* **168**, 107985 (2020).
52. Freund, T. F., Gulyás, A. I., Acsády, L., Görcs, T. & Tóth, K. Serotonergic control of the hippocampus via local inhibitory interneurons. *Proceedings of the National Academy of Sciences* **87**, 8501–8505 (1990).
53. Varga, V. *et al.* Fast synaptic subcortical control of hippocampal circuits. *Science* **326**, 449–453 (2009).

54. Turi, G. F. *et al.* Serotonin modulates infraslow oscillation in the dentate gyrus during Non-REM sleep. *eLife* **13**, (2025).
55. Maru, E., Takahashi, L. K. & Iwahara, S. Effects of median raphe nucleus lesions on hippocampal EEG in the freely moving rat. *Brain Research* **163**, 223–234 (1979).
56. Yamamoto, T., Watanabe, S., Oishi, R. & Ueki, S. Effects of midbrain raphe stimulation and lesion on EEG activity in rats. *Brain Research Bulletin* **4**, 491–495 (1979).
57. Ohmura, Y. *et al.* Serotonin 5-ht $_7$ receptor in the ventral hippocampus modulates the retrieval of fear memory and stress-induced defecation. *Int J Neuropsychopharmacol* (2015) doi:10.1093/ijnp/pyv131.
58. Karayol, R. *et al.* Serotonin receptor 4 in the hippocampus modulates mood and anxiety. *Mol Psychiatry* **26**, 2334–2349 (2021).
59. Alves, S. H., Pinheiro, G., Motta, V., Landeira-Fernandez, J. & Cruz, A. P. M. Anxiogenic effects in the rat elevated plus-maze of 5-HT(2C) agonists into ventral but not dorsal hippocampus. *Behav Pharmacol* **15**, 37–43 (2004).
60. Metzger, M., Bueno, D. & Lima, L. B. The lateral habenula and the serotonergic system. *Pharmacology Biochemistry and Behavior* **162**, 22–28 (2017).
61. Vertes, R. P., Fortin, W. J. & Crane, A. M. Projections of the median raphe nucleus in the rat. *J Comp Neurol* **407**, 555–582 (1999).
62. Amo, R. *et al.* The habenulo-raphe serotonergic circuit encodes an aversive expectation value essential for adaptive active avoidance of danger. *Neuron* **84**, 1034–1048 (2014).
63. Tsao, C.-H., Wu, K.-Y., Su, N. C., Edwards, A. & Huang, G.-J. The influence of sex difference on behavior and adult hippocampal neurogenesis in C57BL/6 mice. *Sci Rep* **13**, 17297 (2023).
64. Rex, A., Voigt, J. P. & Fink, H. Anxiety but not arousal increases 5-hydroxytryptamine release in the rat ventral hippocampus in vivo. *European Journal of Neuroscience* **22**, 1185–1189 (2005).
65. Kusljic, S., Copolov, D. L. & van den Buuse, M. Differential role of serotonergic projections arising from the dorsal and median raphe nuclei in locomotor hyperactivity and prepulse inhibition. *Neuropsychopharmacol* **28**, 2138–2147 (2003).
66. Wirtshafter, D. & Asin, K. E. Evidence that electrolytic median raphe lesions increase locomotion but not exploration. *Physiology & Behavior* **28**, 749–754 (1982).
67. Casarrubea, M. *et al.* Temporal structure of the rat's behavior in elevated plus maze test. *Behavioural Brain Research* **237**, 290–299 (2013).
68. Arabo, A., Potier, C., Ollivier, G., Lorivel, T. & Roy, V. Temporal analysis of free exploration of an elevated plus-maze in mice. *Journal of Experimental Psychology: Animal Learning and Cognition* **40**, 457–466 (2014).
69. Akiti, K. *et al.* Striatal dopamine explains novelty-induced behavioral dynamics and individual variability in threat prediction. *Neuron* **110**, 3789-3804.e9 (2022).
70. Hasselmo, M. E. & Stern, C. E. Theta rhythm and the encoding and retrieval of space and time. *NeuroImage* **85**, 656–666 (2014).
71. Colgin, L. L. Rhythms of the hippocampal network. *Nat Rev Neurosci* **17**, 239–249 (2016).

72. Buzsáki, G. & Moser, E. I. Memory, navigation and theta rhythm in the hippocampal-entorhinal system. *Nat Neurosci* **16**, 130–138 (2013).
73. Whishaw, I. Q. & Vanderwolf, C. H. Hippocampal EEG and behavior: changes in amplitude and frequency of RSA (theta rhythm) associated with spontaneous and learned movement patterns in rats and cats. *Behav Biol* **8**, 461–484 (1973).
74. Hinman, J. R., Penley, S. C., Long, L. L., Escabí, M. A. & Chrobak, J. J. Septotemporal variation in dynamics of theta: speed and habituation. *J Neurophysiol* **105**, 2675–2686 (2011).
75. Jeewajee, A., Lever, C., Burton, S., O'Keefe, J. & Burgess, N. Environmental novelty is signaled by reduction of the hippocampal theta frequency. *Hippocampus* **18**, 340–348 (2008).
76. Kropff, E., Carmichael, J. E., Moser, E. I. & Moser, M.-B. Frequency of theta rhythm is controlled by acceleration, but not speed, in running rats. *Neuron* **109**, 1029-1039.e8 (2021).
77. Wells, C. E. *et al.* Novelty and anxiolytic drugs dissociate two components of hippocampal theta in behaving rats. *J. Neurosci.* **33**, 8650–8667 (2013).
78. Monaghan, C. K., Chapman, G. W. & Hasselmo, M. E. Systemic administration of two different anxiolytic drugs decreases local field potential theta frequency in the medial entorhinal cortex without affecting grid cell firing fields. *Neuroscience* **364**, 60–70 (2017).
79. Hines, M. *et al.* Frequency matters: how changes in hippocampal theta frequency can influence temporal coding, anxiety-reduction, and memory. *Front. Syst. Neurosci.* **16**, 998116 (2023).
80. Ohmura, Y., Tanaka, K. F., Tsunematsu, T., Yamanaka, A. & Yoshioka, M. Optogenetic activation of serotonergic neurons enhances anxiety-like behaviour in mice. *International Journal of Neuropsychopharmacology* **17**, 1777–1783 (2014).
81. Correia, P. A. *et al.* Transient inhibition and long-term facilitation of locomotion by phasic optogenetic activation of serotonin neurons. *Elife* **6**, e20975 (2017).
82. Seo, C. *et al.* Intense threat switches dorsal raphe serotonin neurons to a paradoxical operational mode. *Science* **363**, 538–542 (2019).
83. Konno, K. *et al.* Early postnatal stress affects the serotonergic function in the median raphe nuclei of adult rats. *Brain Res* **1172**, 60–66 (2007).
84. Palanza, P. Animal models of anxiety and depression: how are females different? *Neurosci Biobehav Rev* **25**, 219–233 (2001).
85. Kalueff, A. V. & Tuohimaa, P. The grooming analysis algorithm discriminates between different levels of anxiety in rats: potential utility for neurobehavioural stress research. *Journal of Neuroscience Methods* **143**, 169–177 (2005).
86. Spruijt, B. M., van Hooff, J. A. & Gispen, W. H. Ethology and neurobiology of grooming behavior. *Physiological Reviews* **72**, 825–852 (1992).
87. Kalueff, A. V. *et al.* Neurobiology of rodent self-grooming and its value for translational neuroscience. *Nat Rev Neurosci* **17**, 45–59 (2016).
88. Berridge, K. C. Comparative fine structure of action: Rules of form and sequence in the grooming patterns of six rodent species. *Behaviour* **113**, 21–56 (1990).

89. Köhler, C. & Steinbusch, H. Identification of serotonin and non-serotonin-containing neurons of the mid-brain raphe projecting to the entorhinal area and the hippocampal formation. A combined immunohistochemical and fluorescent retrograde tracing study in the rat brain. *Neuroscience* **7**, 951–975 (1982).
90. McKenna, J. T. & Vertes, R. P. Collateral projections from the median raphe nucleus to the medial septum and hippocampus. *Brain Res Bull* **54**, 619–630 (2001).
91. Jacobs, B. L. & Azmitia, E. C. Structure and function of the brain serotonin system. *Physiol Rev* **72**, 165–229 (1992).
92. Guajardo, H. M., Hatini, P. G. & Commons, K. G. The mouse dorsal raphe nucleus as understood by temporal Fgf8 lineage analysis. *J Comp Neurol* **529**, 2042–2054 (2021).
93. Howerton, A. R. *et al.* Sex differences in corticotropin-releasing factor receptor-1 action within the dorsal raphe nucleus in stress responsivity. *Biol Psychiatry* **75**, 873–883 (2014).
94. Torres Irizarry, V. C. *et al.* Estrogen signaling in the dorsal raphe regulates binge-like drinking in mice. *Transl Psychiatry* **14**, 122 (2024).
95. Jensen, P. *et al.* Redefining the serotonergic system by genetic lineage. *Nat Neurosci* **11**, 417–419 (2008).
96. Senft, R. A., Freret, M. E., Sturrock, N. & Dymecki, S. M. Neurochemically and Hodologically Distinct Ascending VGLUT3 versus Serotonin Subsystems Comprise the r2-Pet1 Median Raphe. *Journal of Neuroscience* **41**, 2581–2600 (2021).
97. Amilhon, B. *et al.* VGLUT3 (Vesicular Glutamate Transporter Type 3) Contribution to the Regulation of Serotonergic Transmission and Anxiety. *Journal of Neuroscience* **30**, 2198–2210 (2010).
98. Fortin-Houde, J., Henderson, F., Dumas, S., Ducharme, G. & Amilhon, B. Parallel streams of raphe VGLUT3-positive inputs target the dorsal and ventral hippocampus in each hemisphere. *J Comp Neurol* **531**, 702–719 (2023).
99. Henderson, F. *et al.* Regulation of stress-induced sleep perturbations by dorsal raphe VGLUT3 neurons in male mice. *Cell Rep* **43**, 114411 (2024).
100. Sengupta, A., Bocchio, M., Bannerman, D. M., Sharp, T. & Capogna, M. Control of Amygdala Circuits by 5-HT Neurons via 5-HT and Glutamate Cotransmission. *J Neurosci* **37**, 1785–1796 (2017).
101. Wang, H.-L. *et al.* Dorsal Raphe Dual Serotonin-Glutamate Neurons Drive Reward by Establishing Excitatory Synapses on VTA Mesoaccumbens Dopamine Neurons. *Cell Rep* **26**, 1128-1142.e7 (2019).
102. Cohen, J. Y., Amoroso, M. W. & Uchida, N. Serotonergic neurons signal reward and punishment on multiple timescales. *Elife* **4**, e06346 (2015).
103. Matias, S., Lottem, E., Dugué, G. P. & Mainen, Z. F. Activity patterns of serotonin neurons underlying cognitive flexibility. *Elife* **6**, e20552 (2017).
104. Zhong, W., Li, Y., Feng, Q. & Luo, M. Learning and Stress Shape the Reward Response Patterns of Serotonin Neurons. *J Neurosci* **37**, 8863–8875 (2017).

105. Sörman, E., Wang, D., Hajos, M. & Kocsis, B. Control of hippocampal theta rhythm by serotonin: Role of 5-HT2c receptors. *Neuropharmacology* **61**, 489–494 (2011).
106. Olvera-Cortés, M. E., Gutiérrez-Guzmán, B. E., López-Loeza, E., Hernández-Pérez, J. J. & López-Vázquez, M. Á. Serotonergic modulation of hippocampal theta activity in relation to hippocampal information processing. *Exp Brain Res* **230**, 407–426 (2013).
107. Vertes, R. P. & Linley, S. B. Chapter 19 - Serotonergic regulation of hippocampal rhythmical activity. in *Handbook of Behavioral Neuroscience* (eds. Müller, C. P. & Cunningham, K. A.) vol. 31 337–360 (Elsevier, 2020).
108. Jackson, J., Dickson, C. T. & Bland, B. H. Median raphe stimulation disrupts hippocampal theta via rapid inhibition and state-dependent phase reset of theta-related neural circuitry. *J Neurophysiol* **99**, 3009–3026 (2008).
109. Lee, A. T. *et al.* VIP interneurons contribute to avoidance behavior by regulating information flow across hippocampal-prefrontal networks. *Neuron* **102**, 1223-1234.e4 (2019).
110. Song, C., Berridge, K. C. & Kalueff, A. V. 'Stressing' rodent self-grooming for neuroscience research. *Nat Rev Neurosci* **17**, 591–591 (2016).
111. Fernández-Teruel, A. & Estanislau, C. Meanings of self-grooming depend on an inverted U-shaped function with aversiveness. *Nat Rev Neurosci* **17**, 591–591 (2016).
112. Tanaka, K. F., Samuels, B. A. & Hen, R. Serotonin receptor expression along the dorsal–ventral axis of mouse hippocampus. *Philos Trans R Soc Lond B Biol Sci* **367**, 2395–2401 (2012).
113. Jin, J. & Maren, S. Fear renewal preferentially activates ventral hippocampal neurons projecting to both amygdala and prefrontal cortex in rats. *Sci Rep* **5**, 8388 (2015).
114. Jimenez, J. C. *et al.* Contextual fear memory retrieval by correlated ensembles of ventral CA1 neurons. *Nat Commun* **11**, 3492 (2020).
115. Gergues, M. M. *et al.* Circuit and molecular architecture of a ventral hippocampal network. *Nat Neurosci* **23**, 1444–1452 (2020).
116. Wee, R. W. S. & MacAskill, A. F. Biased connectivity of brain-wide inputs to ventral subiculum output neurons. *Cell Rep* **30**, 3644-3654.e6 (2020).
117. Paul, E. D. & Lowry, C. A. Functional topography of serotonergic systems supports the Deakin/Graeff hypothesis of anxiety and affective disorders. *J Psychopharmacol* **27**, 1090–1106 (2013).
118. Ravenelle, R. *et al.* Serotonergic Modulation of the BNST-CeA Circuit Promotes Sex Differences in Fear Learning. *bioRxiv* 2023.07.03.547577 (2023) doi:10.1101/2023.07.03.547577.
119. Craske, M. G. & Stein, M. B. Anxiety. *Lancet* **388**, 3048–3059 (2016).
120. Kessler, R. C. *et al.* The global burden of mental disorders: An update from the WHO World Mental Health (WMH) Surveys. *Epidemiol Psichiatr Soc* **18**, 23–33 (2009).
121. Kessler, R. C. *et al.* Lifetime prevalence and age-of-onset distributions of DSM-IV disorders in the National Comorbidity Survey Replication. *Archives of General Psychiatry* **62**, 593–602 (2005).

122. Keevers, L. J. & Jean-Richard-dit-Bressel, P. Obtaining artifact-corrected signals in fiber photometry via isosbestic signals, robust regression, and dF/F calculations. *Neurophotonics* **12**, 025003 (2025).
123. Pereira, T. D. *et al.* SLEAP: A deep learning system for multi-animal pose tracking. *Nat Methods* **19**, 486–495 (2022).
124. Siegle, J. H. *et al.* Open Ephys: an open-source, plugin-based platform for multichannel electrophysiology. *J Neural Eng* **14**, 045003 (2017).
125. Mathis, A. *et al.* DeepLabCut: markerless pose estimation of user-defined body parts with deep learning. *Nature Neuroscience* **21**, 1281–1289 (2018).
126. Nath, T. *et al.* Using DeepLabCut for 3D markerless pose estimation across species and behaviors. *Nat Protoc* **14**, 2152–2176 (2019).
127. Paxinos, G. & Franklin, K. B. J. *Paxinos and Franklin's the Mouse Brain in Stereotaxic Coordinates*. (Academic Press, 2019).
128. Ting, J. T., Daigle, T. L., Chen, Q. & Feng, G. Acute brain slice methods for adult and aging animals: application of targeted patch clamp analysis and optogenetics. *Methods Mol Biol* **1183**, 221–242 (2014).
129. Brown, M. B. & Forsythe, A. B. Robust tests for the equality of variances. *Journal of the American Statistical Association* **69**, 364–367 (1974).

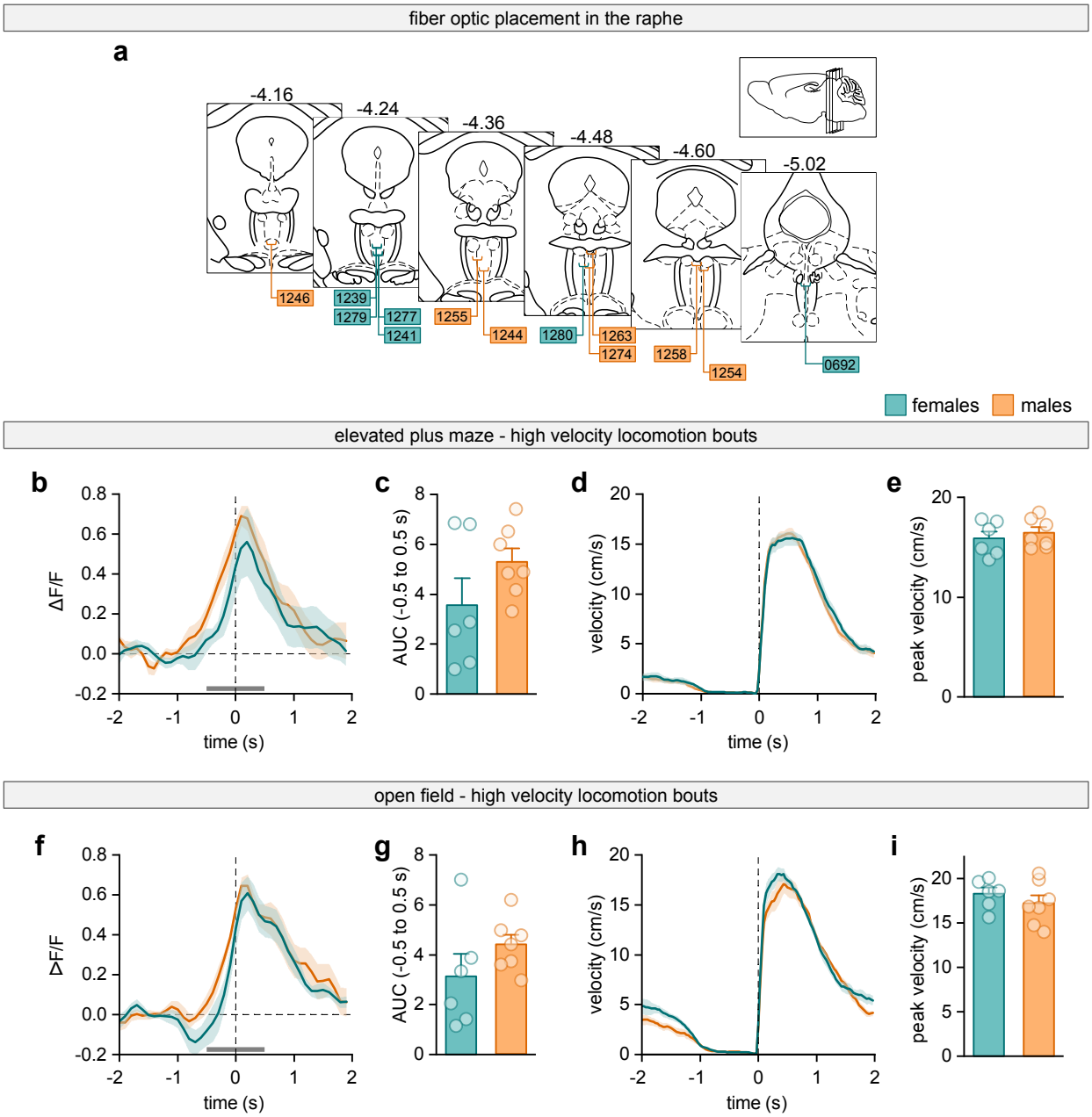

Extended Data Fig. 1: Locomotion-related activity of 5-HT^{vHP} neurons does not differ between sexes. a, Optic fiber placements for all animals used for fiber photometry experiments (n = 6 females, n = 7 males). Numbers in boxes indicate individual animal IDs; brain schematics show distance from bregma in mm. **b,** Mean normalized GCaMP6s fluorescence signal aligned to the initiation of high velocity locomotion bouts for females (teal, n = 6) and males (orange, n = 7) in the EPM. Dotted vertical line: onset of locomotion. Gray bar indicates the period used for panel **c**. **c,** AUC of ΔF/F from –0.5 to +0.5 s around high velocity locomotion onset in the EPM. **d,** Corresponding instantaneous velocity across all detected high velocity locomotion bouts. Dotted vertical line indicates onset of locomotor bout. **e,** Quantification of peak velocity for each animal in **d. f,** Same as **b,** but for the open field. Gray bar indicates the period used for panel **g**. **g,** Same as **c,** but for the open field. **h,** Same as **d,** but for the open field. **i,** Same as **e,** but for the open field. **b** – **i**, all data are shown as mean ± s.e.m. For detailed statistical information, see Extended Data Table 1.

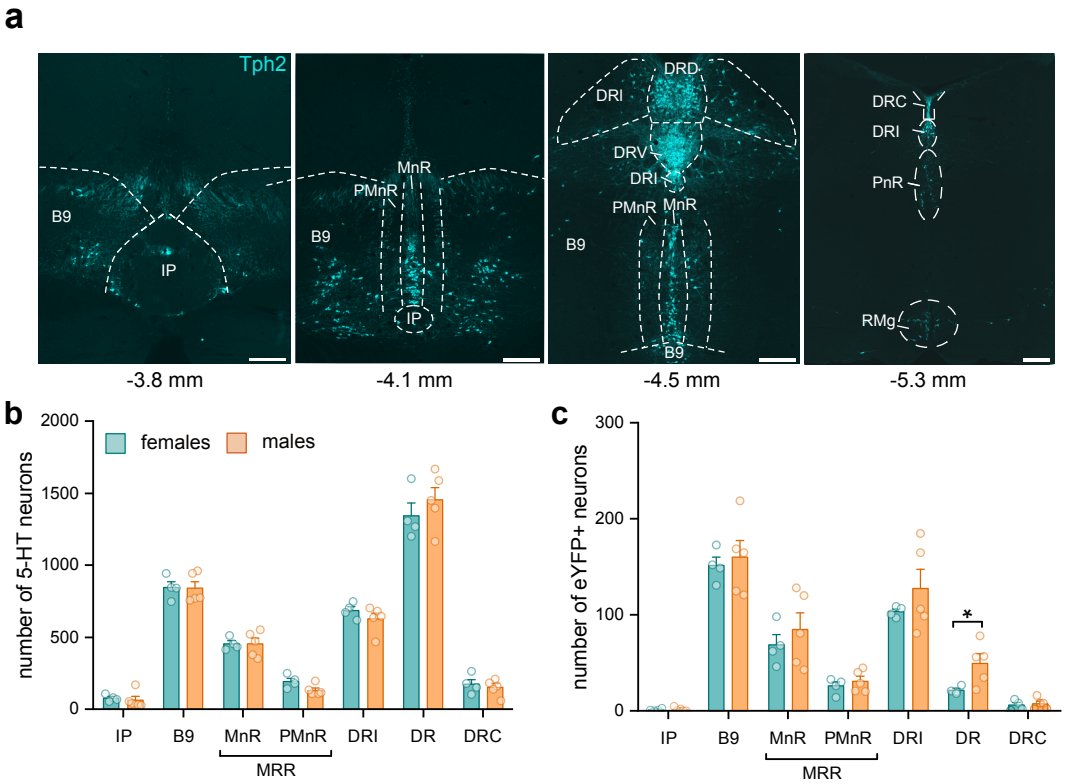

Extended Data Fig. 2: Sex-independent distribution of 5-HT^{vHP} neurons across raphe subregions. a, Schematic delineations of raphe regions with 5-HT+ neurons (Tph2+, blue). Distance from bregma shown in mm. Scale bars = 250 µm. **b,** Total number of 5-HT+ neurons for each raphe subregion, for both sexes (females: n = 4; males: n = 5). **c,** Total number of eYFP+ neurons per subregion, for both sexes. For the DR, two-sample t-test, P = 0.0394. All data are shown as mean ± s.e.m. *: $P < 0.05$. Abbreviations: IP: interpeduncular nucleus, B9: B9 nucleus; MnR: median part of the median raphe region; PMnR: paramedian part of the median raphe region; MRR: median raphe region; DRI: dorsal raphe, interfascicular subregion; DR: dorsal raphe; DRC: caudal part of the dorsal raphe; Tph2: tryptophan hydroxylase type 2; eYFP: enhanced yellow fluorescent protein; For detailed statistical information, see Extended Data Table 1.

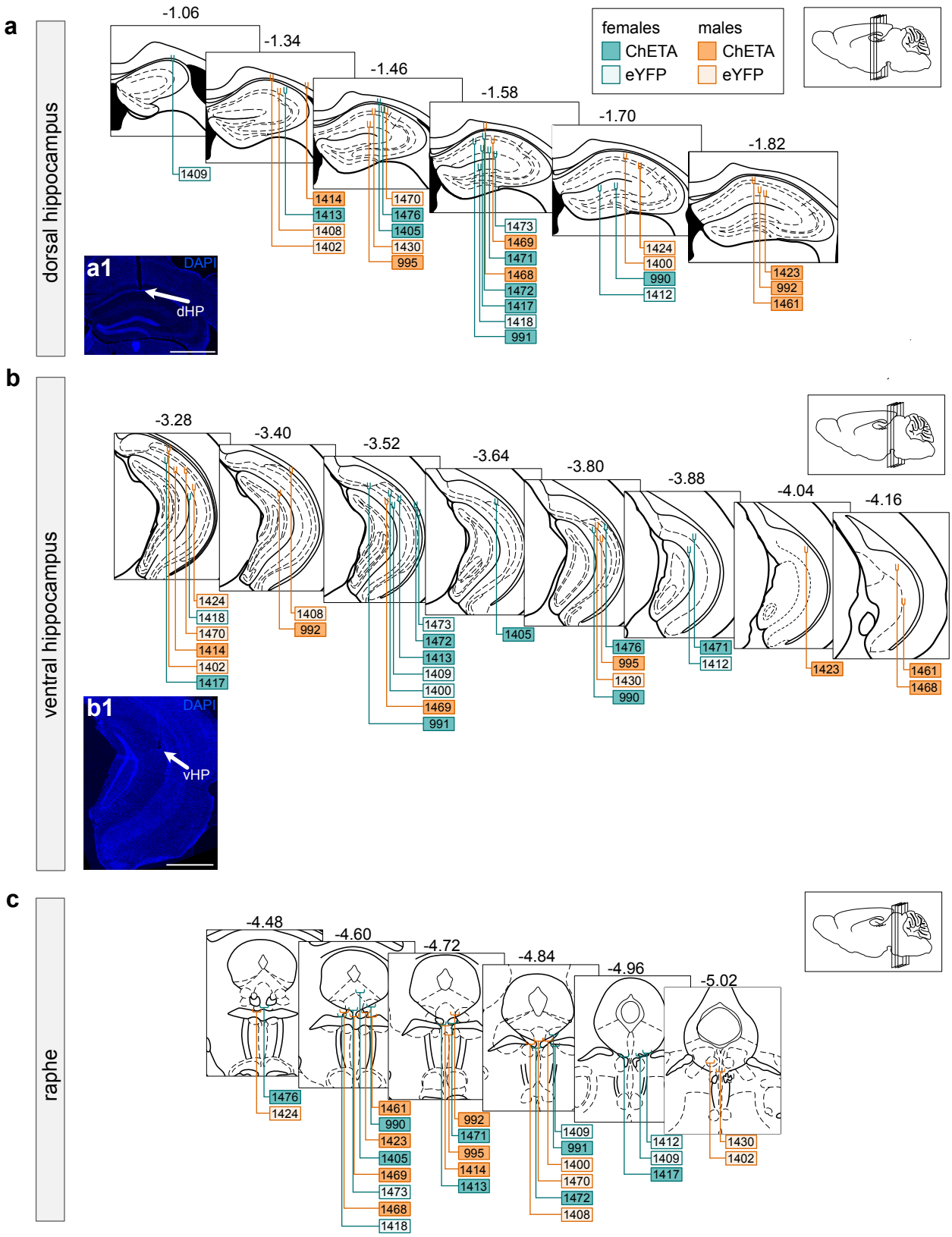

Extended Data Fig. 3: Electrode and optic fiber placements for LFP recordings and optogenetic stimulation. **a,** Approximate electrode placement in the dHP, with representative electrode tract (**a1**, DAPI in blue; as indicated by white arrow). Scale bar = 1000 µm. Numbers in boxes indicate ID of the animals. Numbers above diagrams indicate distance from bregma in mm. **b,** Same as **a**, for the vHP (**b1**: representative tract as indicated by white arrow). Scale bar = 1000 µm. **c,** Fiber optic placement in the raphe.

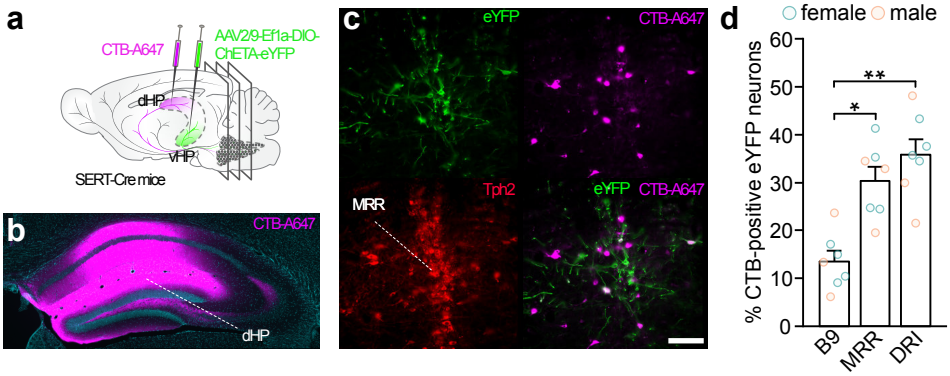

Extended Data Fig. 4: Subpopulation of 5-HT^{vHP} neurons collateralizes to dHP. a, Experimental strategy for dual retrograde labeling of 5-HT^{vHP} neurons projecting to both the dHP and the vHP. **b,** Representative image of CTB-A647 (magenta) in the dHP. **c,** Representative image of triple-labeled 5-HT neurons (Tph2+, red), expressing eYFP (eYFP+, green) and CTB-A647 (CTB+, magenta) in the MRR. Scale bar = 100 µm. **d,** Proportion of double-labeled 5-HT^{vHP} neurons across raphe subregions for females (teal, n = 4) and males (orange, n = 3): 13.39% in B9, 32.83% in the MRR and ≥ 35.71% in the DR. Kruskall-Wallis ANOVA, with Dunn's post-hoc testing. B9 vs MRR: $P = 0.0258$, B9 vs DRI: $P = 0.0017$. Data are shown as mean ± s.e.m. * : $P < 0.05$, ** : $P < 0.01$. CTB: Cholera Toxin Subunit B; dHP: dorsal hippocampus**;** DRI: dorsal raphe, interfascicular subregion; eYFP: enhanced yellow fluorescent protein; MRR: median raphe region; For detailed statistical information, see Extended Data Table 1.

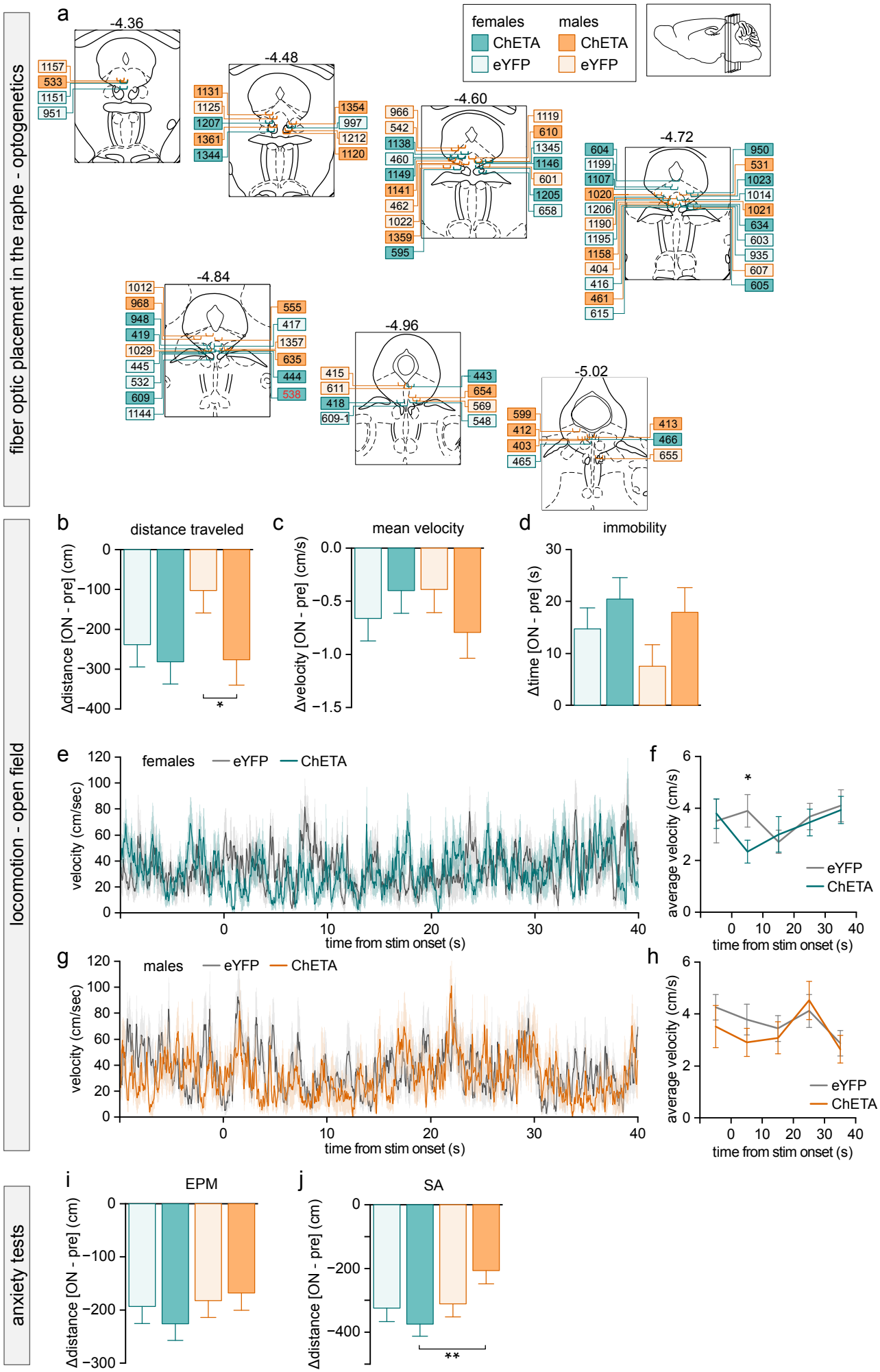
fiber optic placement in the raphe - optogenetics
a
-4.36
-4.48
-4.60
-4.72
-4.84
-4.96
-5.02
females
ChETA
eYFP
males
ChETA
eYFP
locomotion - open field
b
distance traveled
Δdistance [ON - pre] (cm)
c
mean velocity
Δvelocity [ON - pre] (cm/s)
d
immobility
Δtime [ON - pre] (s)
e
females
eYFP
ChETA
velocity (cm/sec)
time from stim onset (s)
f
average velocity (cm/s)
time from stim onset (s)
g
males
eYFP
ChETA
velocity (cm/sec)
time from stim onset (s)
h
average velocity (cm/s)
time from stim onset (s)
anxiety tests
i
EPM
Δdistance [ON - pre] (cm)
j
SA
Δdistance [ON - pre] (cm)

Extended Data Fig. 5: Optogenetic activation of 5-HT^{vHP} neurons does not consistently alter locomotion. a, Fiber optic placement in raphe of experimental mice used for optogenetic stimulation during behavioral tests. Numbers above diagrams indicate distance from bregma in mm. Numbers in boxes indicate identification number of experimental subject. **b,** Difference between the distance travelled during the 4 min of optogenetic stimulation (ON) and the first 4 min of baseline (pre) periods in the open field for each group. No difference was observed for females while ChETA-expressing males showed a modest reduction in distance traveled. Three-way ANOVA with Holms multiple comparison testing: males (ChETA vs control), P = 0.0452). **c,** Same as **b**, but for mean velocity, no difference was observed for either sex. **d,** Same as **b**, but for time spent immobile. Here again, no difference was observed for either sex. **e,** Instantaneous velocity over time, around light stimulation onset (time = 0) for female eYFP (gray) and ChETA (teal) mice in the open field. **f,** Velocity averaged by 10 s bouts, around light stimulation onset (time = 0) for female eYFP (gray) and ChETA (teal) mice in the open field. Time-binned analyses of average velocity confirmed the absence of prominent stimulation effects, aside from a transient (10 s) decrease in average velocity. Two-sample t-test, eYFP vs control, 0 - 10 s, P = 0.0461. **g,** Same as **e**, but for male eYFP (gray) and ChETA (orange) mice. **h,** Same as **f**, but for male eYFP (gray) and ChETA (orange) mice. No change in velocity was observed in males. **i,** Same as **b**, but in the elevated plus maze (EPM). **j,** Same as **b**, but in the successive alleys (SA). Three-way ANOVA with Holms multiple comparison testing, ChETA (female vs male), P = 0.0041. Data are shown as mean ± s.e.m. *: $P < 0.05$, **: $P < 0.01$; For **b-d** and **i-j**, data are from two independent experiments and were analyzed by three-way ANOVA. For detailed statistical information and for the numbers of female and male mice used, see Extended Data Table 1. For an overview of all behavioral variables analyzed, see Extended Data Table 2.

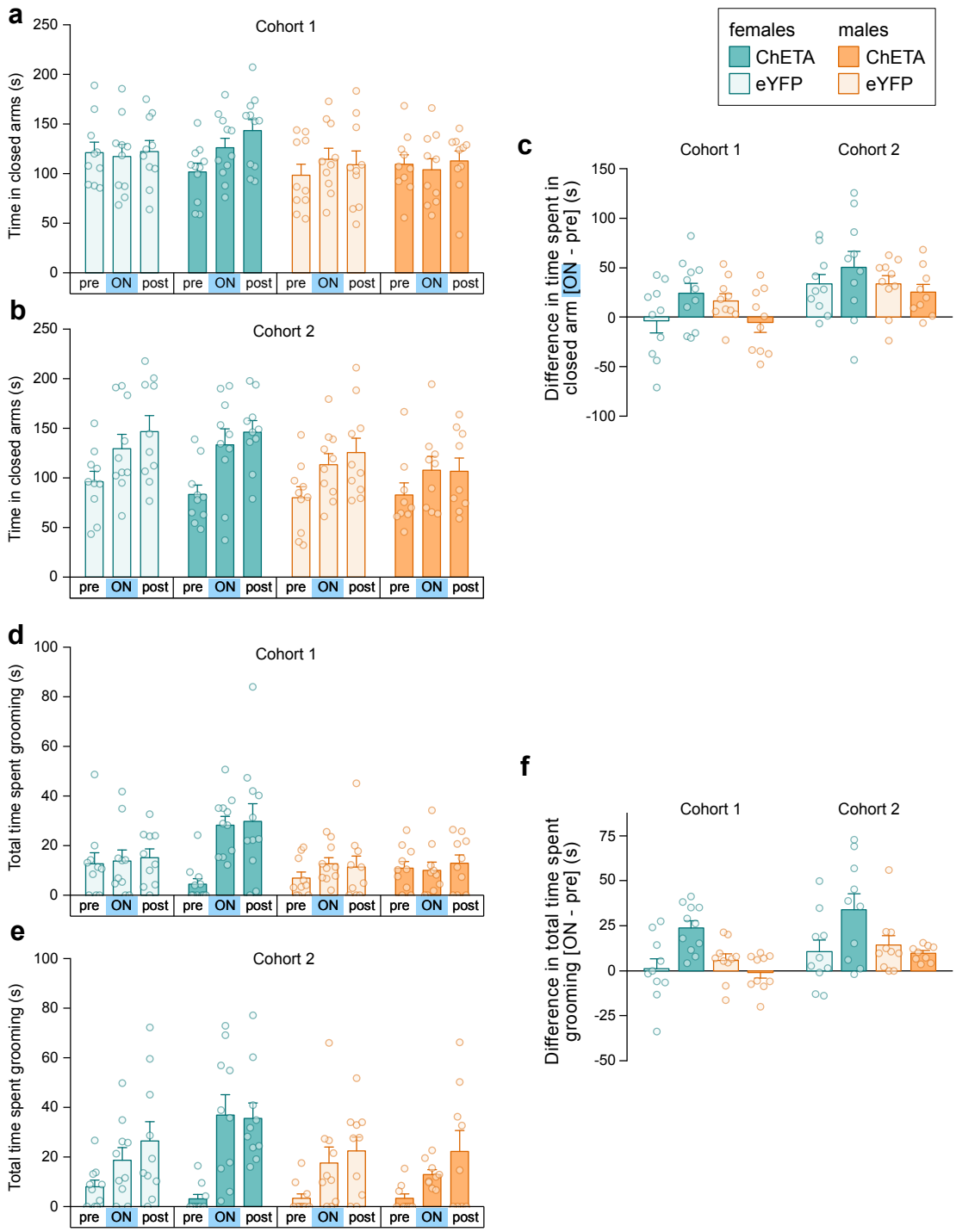

Extended Data Fig. 6: Effects of 5-HT^{vHP} activation on closed-arm time and grooming across cohorts. a,b, Time spent in the closed arms during the pre-stimulation (pre), stimulation (stim) and post-stimulation (post) epochs for cohort 1 (**a**) and cohort 2 (**b**). **c,** Change in closed-arm time for both cohorts. **d,e,** Total time spent grooming during pre, stim and post epochs for cohort 1 (**d**) and cohort 2 (**e**). **f,** Change in grooming time for both cohorts. Data are shown as mean ± s.e.m.

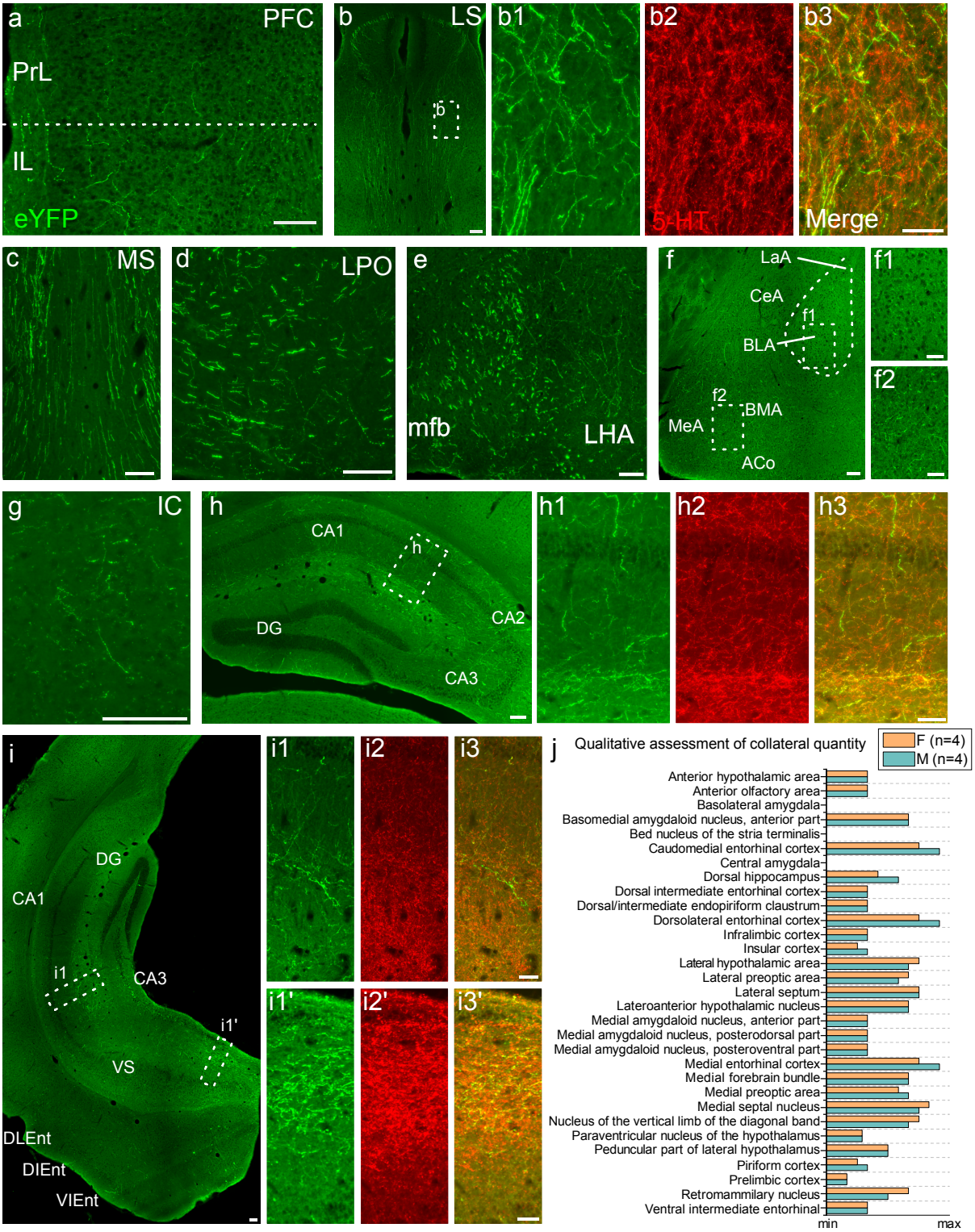

Extended Data Fig. 7: 5-HT^{vHP} collateralization to the forebrain. eYFP-positive collaterals are detected using anti-GFP immunostaining. **a,** Sparse axons in the prefrontal cortex (PFC). **b,** High density of axons present in the lateral septum (LS). Overlay of the eYFP fibers with anti-5-HT immunostaining (b1-b3). **c,** Collaterals are found in the lateral parts of the medial septum (MS). **d,** 5-HT axons are found in the preoptic area with the highest density in the lateral part (LPO). **e,** Axons pass through the medial forebrain bundle (mfb) and a few are observed in the lateral hypothalamic area (LHA). **f,** Medial amygdaloid nucleus (MeA), basomedial amygdaloid nucleus (BMA) and anterior cortical amygdaloid area (ACo) all contain high density of axons while very few to none are observed in the central amygdala (CeA), lateral amygdala (LaA) and the basolateral amygdala (BLA). **g,** Few axons are consistently present in the insular cortex (IC). **h,** The dHP contains 5-HT positive collaterals from neurons targeting its ventral counterpart. **i,** Example of the injection site in the vHP covering the dentate gyrus (DG), CA1, CA3 and VS (ventral subiculum). High density of eYFP labeled axons are present in CA1 (**i1-i3**) and CA3 (**i1'-i3'**). Few axons are observed in the dorsolateral, dorsal intermediate and ventral intermediate part of the entorhinal cortex (DLEnt, DIEnt and VIEnt, respectively) but leakage from the injection site should be considered. **j,** Qualitative assessment of 5-HT collaterals density in female (n = 4) and male (n = 4) mice. Data are shown as mean. ACo: anterior cortical amygdaloid area; BLA: basolateral amygdala; BMA: basomedial amygdaloid nucleus; CeA: central amygdala;

DG: dentate gyrus; DIEnt: dorsal intermediate enthorinal cortex; DLEnt: dorsolateral entorhinal cortex; eYFP: enhanced yellow fluorescent protein; IC: insular cortex; LaA: lateral amygdala; LHA: lateral hypothalamic area; LPO: lateral part of preoptic area; LS: lateral septum; MeA: medial amygdaloid nucleus; mfb: medial forebrain bundle; MS: medial septum; PFC: prefrontal cortex; VIEnt: ventral intermediate part of the entorhinal cortex; VS: ventral subiculum; Scale bar: 100 μm in A-I, 50 μm in b1-b3; f1-f2; h1-h3; i1-i3; i1'-i3'.

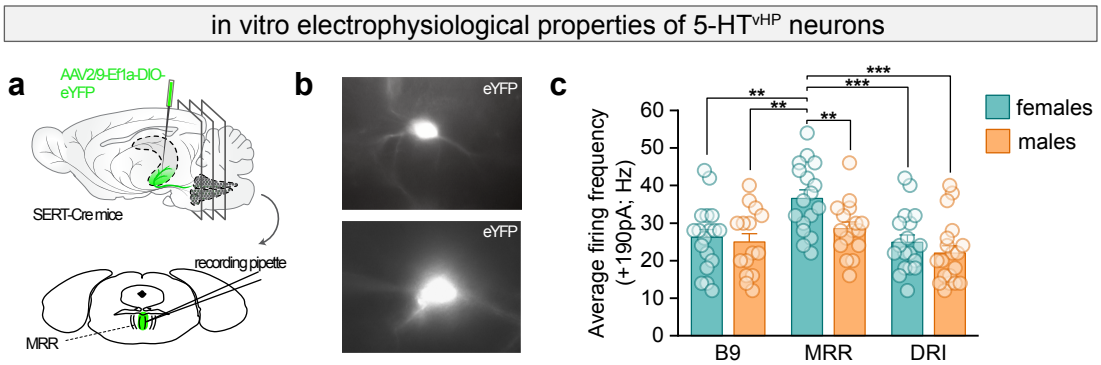

Extended Data Fig. 8: Female MRR 5-HT^{vHP} neurons have the highest firing frequency among all regions and sexes. **a,** Schematic of experimental strategy to assess in-vitro electrophysiological characteristics of 5-HT^{vHP} cells in raphe slices. **b,** Representative examples of eYFP-positive (eYFP+, white) cell. c, Firing frequency at +190 pA. Two sample t-tests, MRR: female vs male, P = 0.0089; Female B9 vs MRR, P = 0.0017; Female MRR vs DRI, P = 0.0003; Female MRR vs male DRI, P = 0.0010; Female MRR vs Male B9, P < 0.0001. All data are shown as mean ± s.e.m; ** : P < 0.01, *** : P = < 0.001*;* For detailed statistical information and for the numbers of female and male mice used, see Extended Data Table 1.

Extended Data Table 1: Summary of statistical analyses					
Fig. 1					
e	AUC closed - open transitions, female (n = 6) vs. male (n = 7)	two-sample t-test		t(11) = 0.9337	p = 0.3705
g	AUC closed - closed transitions, female (n = 6) vs. male (n = 4)	two-sample t-test		t(8) = 0.3928	p = 0.7047
j	AUC closed arm entry, female (n = 6) vs. male (n = 7)	two-sample t-test		t(11) = 2.2865	p = 0.0430*
l	peak velocity closed arm entry, female (n = 6) vs. male (n = 7)	two-sample t-test		t(11) = 0.6583	p = 0.5239
n	AUC closed arm exit, female (n = 6) vs. male (n = 7)	two-sample t-test		t(11) = 0.4194	p = 0.6830
p	peak velocity closed arm exit, female (n = 6) vs. male (n = 7)	two-sample t-test		t(11) = 0.6730	p = 0.5148
s	UAC of change dF/F, female (n = 6) vs. male (n = 7)	two-sample t-test		t(11) = -2.5212	p = 0.0284*
Fig. 2					
c	B9 % eYFP+ 5-HT neurons (n = 4 females, n = 5 males)	two-sample t-test		t(7) = -0.5721	p = 0.5851
	MRR % eYFP+ 5-HT neurons (n = 4 females, n = 5 males)	two-sample t-test		t(7) = -1.4375	p = 0.1937
	DRI % eYFP+ 5-HT neurons (n = 4 females, n = 5 males)	two-sample t-test		t(7) = -1.5153	p = 0.1735
o	delta slope dHP: female eYFP (n = 5); female ChETA (n = 8); male eYFP (n = 5); male ChETA (n = 7);	two-way ANOVA	Main effect of sex	F(1,21) = 0.0131	p = 0.9098
			Main effect of opsin	F(1,21) = 13.5057	p = 0.0014**
			Interaction effect: sex * opsin	F(1,21) = 3.0903	p = 0.0933
		two-sample t-test	Females: eYFP vs. ChETA	t(11) = 4.1395	p = 0.0016**
			Males: eYFP vs. ChETA	t(10) = 1.2604	p = 0.2361
p	delta intercept dHP [ON - pre]: female eYFP (n = 5); female ChETA (n = 8); male eYFP (n = 5); male ChETA (n = 7);	two-way ANOVA	Main effect of sex	F(1,21) = 2.8158	p = 0.1082
			Main effect of opsin	F(1,21) = 3.2462	p = 0.0860
			Interaction effect: sex * opsin	F(1,21) = 1.324	p = 0.2628
		two-sample t-test	Females: eYFP vs. ChETA	t(11) = -2.5343	p = 0.0278*
			Males: eYFP vs. ChETA	t(10) = -0.3935	p = 0.7022
q	delta slope vHP [ON - pre]: female eYFP (n = 5); female ChETA (n = 8); male eYFP (n = 5); male ChETA (n = 7);	two-way ANOVA	Main effect of sex	F(1,21) = 0.2040	p = 0.6562
			Main effect of opsin	F(1,21) = 7.6083	p = 0.0118*
			Interaction effect: sex * opsin	F(1,21) = 0.7837	p = 0.3860
		two-sample t-test	Females: eYFP vs. ChETA	t(11) = 2.5901	p = 0.0251*
			Males: eYFP vs. ChETA	t(10) = 1.3192	p = 0.2165

r	Δ intercept vHP [ON - pre]: female eYFP (n = 5); female ChETA (n = 8); male eYFP (n = 5); male ChETA (n = 7);	two-way ANOVA	Main effect of sex	F(1,21) = 1.9196	p = 0.1804
			Main effect of opsin	F(1,21) = 5.8653	p = 0.0246*
			Interaction effect: sex * opsin	F(1,21) = 0.8650	p = 0.3629
		two-sample t-test	Females: eYFP vs. ChETA	t(11) = -2.6445	p = 0.0228*
			Males: eYFP vs. ChETA	t(10) = -0.9535	p = 0.3628
Fig. 3					
c	EPM delta time in closed arms [ON - pre]: female eYFP (n = 20); female ChETA (n = 21); male eYFP (n = 20); male ChETA (n = 19);	three-way ANOVA	Main effect of sex	F(1,72) = 1.3487	p = 0.2493
			Main effect of opsin	F(1,72) = 0.1956	p = 0.6596
			Main effect of cohort	F(1,72) = 13.3810	p = 0.0005***
			Interaction effect: sex x opsin	F(1,72) = 6.2037	p = 0.0151*
			Interaction effect: sex x cohort	F(1,72) = 0.2751	p = 0.6016
			Interaction effect: treatment x cohort	F(1,72) = 0.0039	p = 0.9501
			Interaction effect: sex x opsin x cohort	F(1,72) = 0.6777	p = 0.4131
		multiple comparisons	Females: eYFP vs. ChETA	t(1,72) = -2.1164	p = 0.0378*
			Males: eYFP vs. ChETA	t(1,72) = 1.4022	p = 0.1652
			eYFP: female vs male	t(1,72) = 0.9497	p = 0.3454
			ChETA: female vs male	t(1,72) = 2.5576	p = 0.0126*
d	EPM delta entries in open arms [ON - pre]: female eYFP (n = 20); female ChETA (n = 21); male eYFP (n = 20); male ChETA (n = 19);	three-way ANOVA	Main effect of sex	F(1,72) = 1.9650	p = 0.1653
			Main effect of opsin	F(1,72) = 1.2348	p = 0.2702
			Main effect of cohort	F(1,72) = 2.5637	p = 0.1137
			Interaction effect: sex x opsin	F(1,72) = 4.4317	p = 0.0388*
			Interaction effect: sex x cohort	F(1,72) = 0.1735	p = 0.6782
			Interaction effect: treatment x cohort	F(1,72) = 0.2375	p = 0.6275
			Interaction effect: sex x opsin x cohort	F(1,72) = 4.0661	p = 0.0475*
		multiple comparisons	Females: eYFP vs. ChETA	t(72) = 2.2450	p = 0.0278*
			Males: eYFP vs. ChETA	t(72) = -0.6651	p = 0.5081
			eYFP: female vs male	t(72) = 0.5172	p = 0.6066
			ChETA: female vs male	t(72) = -2.3704	p = 0.0204*
e	SA occupancy score [ON - pre]: female eYFP (n = 19); female ChETA (n = 20); male eYFP (n = 19); male ChETA (n = 19);	three-way ANOVA	Main effect of sex	F(1,70) = 9.2391	p = 0.0033**
			Main effect of opsin	F(1,70) = 0.1739	p = 0.6780
			Main effect of cohort	F(1,70) = 0.9063	p = 0.3444
			Interaction effect: sex x opsin	F(1,70) = 0.2937	p = 0.5896
			Interaction effect: sex x cohort	F(1,70) = 0.5458	p = 0.4625
			Interaction effect: treatment x cohort	F(1,70) = 0.8867	p = 0.3496
			Interaction effect: sex x opsin x cohort	F(1,70) = 0.8979	p = 0.3466
		multiple comparisons	Females: eYFP vs. ChETA	t(70) = -0.7436	p = 0.4596
			Males: eYFP vs. ChETA	t(70) = 0.0902	p = 0.9284
			eYFP: female vs male	t(70) = 1.6602	p = 0.1014
			ChETA: female vs male	t(70) = 2.5374	p = 0.0134*

f	SA delta number of entries in the open zones [ON - pre]: female eYFP (n = 16); female ChETA (n = 19); male eYFP (n = 17); male ChETA (n = 16);	three-way ANOVA	Main effect of sex	F(1,60) = 1.4382	p = 0.2352
			Main effect of opsin	F(1,60) = 1.7343	p = 0.1929
			Main effect of cohort	F(1,60) = 2.1798	p = 0.1451
			Interaction effect: sex x opsin	F(1,60) = 4.5975	p = 0.0361*
			Interaction effect: sex x cohort	F(1,60) = 0.8330	p = 0.3651
			Interaction effect: treatment x cohort	F(1,60) = 0.1805	p = 0.6724
			Interaction effect: sex x opsin x cohort	F(1,60) = 0.0498	p = 0.8242
		multiple comparisons	Females: eYFP vs. ChETA	t(60) = 2.4274	p = 0.0182*
			Males: eYFP vs. ChETA	t(60) = -0.4569	p = 0.6469
			eYFP: female vs male	t(60) = 0.5834	p = 0.5618
			ChETA: female vs male	t(60) = -2.3219	p = 0.0237*
g	EPM delta number of headdips [ON - pre]: female eYFP (n = 20); female ChETA (n = 21); male eYFP (n = 20); male ChETA (n = 19);	three-way ANOVA	Main effect of sex	F(1,72) = 1.6705	p = 0.2003
			Main effect of opsin	F(1,72) = 1.6098	p = 0.2086
			Main effect of cohort	F(1,72) = 15.2979	p = 0.0002***
			Interaction effect: sex x opsin	F(1,72) = 7.5064	p = 0.0077**
			Interaction effect: sex x cohort	F(1,72) = 0.0600	p = 0.8072
			Interaction effect: treatment x cohort	F(1,72) = 0.3494	p = 0.5563
			Interaction effect: sex x opsin x cohort	F(1,72) = 0.4747	p = 0.4930
		multiple comparisons	Females: eYFP vs. ChETA	t(72) = 2.8843	p = 0.0052**
			Males: eYFP vs. ChETA	t(72) = -0.9774	p = 0.3316
			eYFP: female vs male	t(72) = 1.0478	p = 0.2982
			ChETA: female vs male	t(72) = -2.7874	p = 0.0068**
h	EPM delta number of stretchings [ON - pre]: female eYFP (n = 20); female ChETA (n = 21); male eYFP (n = 20); male ChETA (n = 19);	three-way ANOVA	Main effect of sex	F(1,72) = 4.8322	p = 0.0311*
			Main effect of opsin	F(1,72) = 13.3137	p = 0.0005***
			Main effect of cohort	F(1,72) = 0.9419	p = 0.3350
			Interaction effect: sex x opsin	F(1,72) = 18.2579	p = <0. 0001***
			Interaction effect: sex x cohort	F(1,72) = 1.039	p = 0.3114
			Interaction effect: treatment x cohort	F(1,72) = 0.0445	p = 0.8335
			Interaction effect: sex x opsin x cohort	F(1,72) = 4.1107	p = 0.0463
		multiple comparisons	Females: eYFP vs. ChETA	t(72) = 5.5564	p < 0.0001***
			Males: eYFP vs. ChETA	t(72) = -0.4397	p = 0.6614
			eYFP: female vs male	t(72) = 1.5301	p = 0.1304
			ChETA: female vs male	t(72) = -4.3975	p = 0.0001***

i	SA delta number of headdips [ON - pre]: female eYFP (n = 17); female ChETA (n = 19); male eYFP (n = 17); male ChETA (n = 16);	three-way ANOVA	Main effect of sex	F(1,61) = 8.9432	p = 0.0040**
			Main effect of opsin	F(1,61) = 0.0674	p = 0.7961
			Main effect of cohort	F(1,61) = 01.6633	p = 0.2020
			Interaction effect: sex x opsin	F(1,61) = 4.0286	p = 0.0492*
			Interaction effect: sex x cohort	F(1,61) = 0.0001	p = 0.9907
			Interaction effect: treatment x cohort	F(1,61) = 2.7455	p = 0.1027
			Interaction effect: sex x opsin x cohort	F(1,61) = 0.4552	p = 0.5024
		multiple comparisons	Females: eYFP vs. ChETA	t(61) = 1.7202	p = 0.0905
			Males: eYFP vs. ChETA	t(61) = -1.1949	p = 0.2367
			eYFP: female vs male	t(61) = -0.5438	p = 0.5885
			ChETA: female vs male	t(61) = -3.4904	p = 0.0009***
j	SA delta number of stretchings [ON - pre]: female eYFP (n = 17); female ChETA (n = 19); male eYFP (n = 17); male ChETA (n = 16);	three-way ANOVA	Main effect of sex	F(1,61) = 8.8490	p = 0.0042**
			Main effect of opsin	F(1,61) = 8.8884	p = 0.0041**
			Main effect of cohort	F(1,61) = 1.9296	p = 0.1698
			Interaction effect: sex x opsin	F(1,61) = 1.4374	p = 0.2352
			Interaction effect: sex x cohort	F(1,61) = 1.7785	p = 0.1873
			Interaction effect: treatment x cohort	F(1,61) = 2.2549	p = 0.1383
			Interaction effect: sex x opsin x cohort	F(1,61) = 3.4604	p = 0.0677
		multiple comparisons	Females: eYFP vs. ChETA	t(61) = 2.1362	p = 0.0026**
			Males: eYFP vs. ChETA	t(61) = 1.1199	p = 0.2671
			eYFP: female vs male	t(61) = -1.0335	p = 0.3055
			ChETA: female vs male	t(61) = -2.9972	p = 0.0039**
Fig. 4					
f	AUC grooming start (n = 6 females, n = 7 males)	two-sample t-test		t(11) = -0.2107	p = 0.8369
g	AUC grooming end transitions (n = 6 females, n = 7 males)	two-sample t-test		t(11) = -0.4175	p = 0.6843
h	EPM delta time spent grooming [ON - pre]: female eYFP (n = 20); female ChETA (n = 21); male eYFP (n = 20); male ChETA (n = 19);	three-way ANOVA	Main effect of sex	F(1,72) = 7.7191	p = 0.0070**
			Main effect of opsin	F(1,72) = 5.5207	p = 0.0215*
			Main effect of cohort	F(1,72) = 6.8129	p = 0.0110*
			Interaction effect: sex x opsin	F(1,72) = 14.8490	p = 0.0003***
			Interaction effect: sex x cohort	F(1,72) = 0.0019	p = 0.9657
			Interaction effect: treatment x cohort	F(1,72) = 0.0254	p = 0.8739
			Interaction effect: sex x opsin x cohort	F(1,72) = 0.0084	p = 0.9273
		multiple comparisons	Females: eYFP vs. ChETA	t(72) = -4.4187	p < 0.0001***
			Males: eYFP vs. ChETA	t(72) = 1.0679	p = 0.2891
			eYFP: female vs male	t(72) = -0.8018	p = 0.4253
			ChETA: female vs male	t(72) = 4.6374	p < 0.0001***

i	SA delta time spent grooming [ON - pre]: female eYFP (n = 17); female ChETA (n = 19); male eYFP (n = 17); male ChETA (n = 16);	three-way ANOVA	Main effect of sex	F(1,61) = 9.1382	p = 0.0037**
			Main effect of opsin	F(1,61) = 4.6362	p = 0.0353*
			Main effect of cohort	F(1,61) = 1.9376	p = 0.1690
			Interaction effect: sex x opsin	F(1,61) = 0.9183	p = 0.3417
			Interaction effect: sex x cohort	F(1,61) = 0.6051	p = 0.4396
			Interaction effect: treatment x cohort	F(1,61) = 0.0211	p = 0.8849
			Interaction effect: sex x opsin x cohort	F(1,61) = 0.5924	p = 0.4444
		multiple comparisons	Females: eYFP vs. ChETA	t(61) = -2.2005	p = 0.0316*
			Males: eYFP vs. ChETA	t(61) = -0.8860	p = 0.3791
			eYFP: female vs male	t(61) = 1.3760	p = 0.1738
			ChETA: female vs male	t(61) = 2.6646	p = 0.0098**
j	OF delta time spent grooming [ON - pre]: female eYFP (n = 19); female ChETA (n = 19); male eYFP (n = 18); male ChETA (n = 15);	three-way ANOVA	Main effect of sex	F(1,63) = 0.0080	p = 0.9292
			Main effect of opsin	F(1,63) = 0.3102	p = 0.5795
			Main effect of cohort	F(1,63) = 4.1558	p = 0.0457*
			Interaction effect: sex x opsin	F(1,63) = 0.0361	p = 0.8498
			Interaction effect: sex x cohort	F(1,63) = 1.1635	p = 0.2849
			Interaction effect: treatment x cohort	F(1,63) = 0.9285	p = 0.3389
			Interaction effect: sex x opsin x cohort	F(1,63) = 0.0016	p = 0.9679
		multiple comparisons	Females: eYFP vs. ChETA	t(63) = -0.5049	p = 0.6154
			Males: eYFP vs. ChETA	t(63) = -0.6064	p = 0.5464
			eYFP: female vs male	t(63) = 0.1831	p = 0.8553
			ChETA: female vs male	t(63) = 0.0308	p = 0.9755
Fig. 5					
c	B9 firing frequency: female (n = 18 cells from 9 mice); male (n = 15 cells from 10 mice)	two-sample t-test		t(31) = 0.4206	p = 0.6770
d	B9 RMP: female (n = 18 cells from 9 mice); male (n = 15 cells from 10 mice)	two-sample t-test		t(31) = -1.3372	p = 0.1909
e	B9 input resistance: female (n = 18 cells from 9 mice); male (n = 15 cells from 10 mice)	two-sample t-test		t(31) = 1.1994	p = 0.2394
f	B9 adaptation index: female (n = 18 cells from 9 mice); male (n = 15 cells from 10 mice)	two-sample t-test		t(31) = -0.4924	p = 0.6259
i	MRR firing frequency: female (n = 17 cells from 6 mice); male (n = 16 cells from 6 mice)	two-sample t-test		t(31) = 2.7908	p = 0.0089**
j	MRR RMP: female (n = 17 cells from 6 mice); male (n = 16 cells from 6 mice)	two-sample t-test		t(31) = 2.8375	p = 0.0079**

k	MRR input resistance: female (n = 17 cells from 6 mice); male (n = 16 cells from 6 mice)	two-sample t-test		t(31) = 0.0061	p = 0.9951
l	MRR adaptation index: female (n = 17 cells from 6 mice); male (n = 16 cells from 6 mice)	two-sample t-test		t(31) = -2.4017	p = 0.0225*
o	DRI firing frequency: female (n = 18 cells from 9 mice); male (n = 19 cells from 10 mice)	two-sample t-test		t(36) = 1.2508	p = 0.2191
p	DRI RMP: female (n = 18 cells from 9 mice); male (n = 19 cells from 10 mice)	two-sample t-test		t(36) = 2.4189	p = 0.0207*
q	DRI input resistance: female (n = 18 cells from 9 mice); male (n = 19 cells from 10 mice)	two-sample t-test		t(36) = -0.5412	p = 0.5917
r	DRI adaptation index: female (n = 18 cells from 9 mice); male (n = 19 cells from 10 mice)	two-sample t-test		t(36) = -0.8134	p = 0.4215
t	B9: % cfos+ 5-HTvHP neurons, female eYFP (n = 5); female ChETA (n = 8); male eYFP (n = 5); male ChETA (n = 7);	two-way ANOVA	Main effect of sex	F(1,24) = 1.1394	p = 0.2964
			Main effect of opsin	F(1,24) = 122.0136	p < 0.0001***
			Interaction effect: sex * opsin	F(1,24) = 0.0269	p = 0.8712
		two-sample t-test	Females: eYFP vs. ChETA	t(12) = 7.5767	p < 0.0001***
			Males: eYFP vs. ChETA	t(12) = 8.0862	p < 0.0001***
	MRR: % cfos+ 5-HTvHP neurons, female eYFP (n = 5); female ChETA (n = 8); male eYFP (n = 5); male ChETA (n = 7);	two-way ANOVA	Main effect of sex	F(1,24) = 2.8714	p = 0.1031
			Main effect of opsin	F(1,24) = 102.0638	p < 0.0001***
			Interaction effect: sex * opsin	F(1,24) = 31.2186	p < 0.0001***
		two-sample t-test	Females: eYFP vs. ChETA	t(12) = -12.0044	p < 0.0001***
			Males: eYFP vs. ChETA	t(12) = -2.9827	p = 0.0114*
	DRI: % cfos+ 5-HTvHP neurons, female eYFP (n = 5); female ChETA (n = 8); male eYFP (n = 5); male ChETA (n = 7);	two-way ANOVA	Main effect of sex	F(1,24) = 3.7020	p = 0.0663
			Main effect of opsin	F(1,24) = 265.3516	p < 0.0001***
			Interaction effect: sex * opsin	F(1,24) = 3.1178	p = 0.0902
		two-sample t-test	Females: eYFP vs. ChETA	t(12) = - 13.0058	p < 0.0001***
			Males: eYFP vs. ChETA	t(12) = -10.0881	p < 0.0001***
u	B9	one-sample t-test		t(24) = 0.1639	p = 0.8712
	MRR	one-sample t-test		t(24) = 5.8003	p < 0.0001***
	DRI	one-sample t-test		t(24) = 1.7657	p = 0.0902
Extended Data Fig. 1					
c	AUC closed - open transitions (n = 6 females, n = 7 males)	two-sample t-test		t(11) = -1.5215	p = 0.1563
e	AUC closed - closed transitions (n = 6 females, n = 7 males)	two-sample t-test		t(11) = -0.5857	p = 0.5698
g	AUC closed arm entry (n = 6 females, n = 7 males)	two-sample t-test		t(11) = -1.3444	p = 0.2059

i	peak velocity closed arm entry (n = 6 females, n = 7 males)	two-sample t-test	t(11) = 0.9250	p = 0.3748
Extended Data Fig. 2				
b	IP: number of 5-HT neurons, female (n = 4) vs. male (n = 5)	two-sample t-test	t(7) = 0.3916	p = 0.7070
	B9: number of 5-HT neurons, female (n = 4) vs. male (n = 5)	two-sample t-test	t(7) = 0.0462	p = 0.9645
	MnR: number of 5-HT neurons, female (n = 4) vs. male (n = 5)	two-sample t-test	t(7) = -0.0176	p = 0.9865
	PMnR: number of 5-HT neurons, female (n = 4) vs. male (n = 5)	two-sample t-test	t(7) = 2.2702	p = 0.0575
	DRI: number of 5-HT neurons, female (n = 4) vs. male (n = 5)	two-sample t-test	t(7) = 1.1279	p = 0.2965
	DR: number of 5-HT neurons, female (n = 4) vs. male (n = 5)	two-sample t-test	t(7) = -0.8728	p = 0.4117
	DRC: number of 5-HT neurons, female (n = 4) vs. male (n = 5)	two-sample t-test	t(7) = 0.5334	p = 0.6103
c	IP: number of eYFP+ neurons, female (n = 4) vs. male (n = 5)	two-sample t-test	t(7) = -0.1209	p = 0.9072
	B9: number of eYFP+ neurons, female (n = 4) vs. male (n = 5)	two-sample t-test	t(7) = -0.3968	p = 0.7033
	MnR: number of eYFP+ neurons, female (n = 4) vs. male (n = 5)	two-sample t-test	t(7) = -0.7368	p = 0.4852
	PMnR: number of eYFP+ neurons, female (n = 4) vs. male (n = 5)	two-sample t-test	t(7) = -0.7767	p = 0.4628
	DRI: number of eYFP+ neurons, female (n = 4) vs. male (n = 5)	two-sample t-test	t(7) = -1.0297	p = 0.3374
	DR: number of eYFP+ neurons, female (n = 4) vs. male (n = 5)	two-sample t-test	t(7) = -2.5278	p = 0.0394*
	DRC: number of eYFP+ neurons, female (n = 4) vs. male (n = 5)	two-sample t-test	t(7) = -0.4557	p = 0.6624

Extended Data Fig. 4					
d	% CTB+ eYFP+ neurons: B9 female (n = 4), male (n = 3); MRR female (n = 4), male (n = 3); DRI female (n = 4), male (n = 3)	KWANOVA		$\chi^2(2) = 12.9648$	p = 0.0015**
		Dunn's test	B9 vs MRR	Z = -2.6274	p = 0.0258*
			B9 vs DRI	Z = -3.4458	p = 0.0017**
			MRR vs DRI	Z = -0.8184	p = 1.0000
Extended Data Fig. 5					
b	delta total distance travelled in OF [ON - pre]: female eYFP (n = 19); female ChETA (n = 19); male eYFP (n = 18); male ChETA (n = 15);	three-way ANOVA	Main effect of sex	F(1,63) = 1.7990	p = 0.1847
			Main effect of opsin	F(1,63) = 2.4494	p = 0.1226
			Main effect of cohort	F(1,63) = 13.8569	p = 0.0004***
			Interaction effect: sex x opsin	F(1,63) = 1.1764	p = 0.2822
			Interaction effect: sex x cohort	F(1,63) = 0.8831	p = 0.3509
			Interaction effect: treatment x cohort	F(1,63) = 0.0517	p = 0.8209
			Interaction effect: sex x opsin x cohort	F(1,63) = 1.5216	p = 0.2220
		multiple comparisons	Females: eYFP vs. ChETA	t(63) = 0.5382	p = 0.5923
			Males: eYFP vs. ChETA	t(63) = 2.0432	p = 0.0452*
			eYFP: female vs male	t(63) = -1.7189	p = 0.0905
			ChETA: female vs male	t(63) = -0.0547	p = 0.9565
c	delta velocity in OF [ON - pre]: female eYFP (n = 19); female ChETA (n = 19); male eYFP (n = 18); male ChETA (n = 15);	three-way ANOVA	Main effect of sex	F(1,63) = 0.0152	p = 0.9022
			Main effect of opsin	F(1,63) = 0.0066	p = 0.9356
			Main effect of cohort	F(1,63) = 9.1314	p = 0.0036**
			Interaction effect: sex x opsin	F(1,63) = 1.9551	p = 0.1669
			Interaction effect: sex x cohort	F(1,63) = 0.4372	p = 0.5109
			Interaction effect: treatment x cohort	F(1,63) = 1.1736	p = 0.2828
			Interaction effect: sex x opsin x cohort	F(1,63) = 0.3692	p = 0.5456
		multiple comparisons	Females: eYFP vs. ChETA	t(63) = -0.8705	p.= 0.3873
			Males: eYFP vs. ChETA	t(63) = 1.2384	p = 0.2202
			eYFP: female vs male	t(63) = -0.8999	p = 0.3716
			ChETA: female vs male	t(63) = 1.2129	p = 0.2297

d	delta time immobile in OF [ON - pre]: female eYFP (n = 19); female ChETA (n = 19); male eYFP (n = 18); male ChETA (n = 15);	three-way ANOVA	Main effect of sex	F(1,63) = 1.5327	p = 0.2203
			Main effect of opsin	F(1,63) = 2.7391	p = 0.1029
			Main effect of cohort	F(1,63) = 10.5698	p = 0.0018**
			Interaction effect: sex x opsin	F(1,63) = 0.2634	p = 0.6069
			Interaction effect: sex x cohort	F(1,63) = 1.1163	p = 0.2948
			Interaction effect: treatment x cohort	F(1,63) = 0.0001	p = 0.9939
			Interaction effect: sex x opsin x cohort	F(1,63) = 1.4160	p = 0.2385
		multiple comparisons (deails)	ChETA: female vs male	t(63) = -0.9889	p = 0.3265
			Males: eYFP vs. ChETA	t(63) = -1.6707	p = 0.0997
			eYFP: female vs male	t(63) = 1.2430	p = 0.2185
			ChETA: female vs male	t(63) = 0.4029	p = 0.6884
f	binned velocity : female eYFP (n = 19); female ChETA (n =19)	two-sample t-test	females: eYFP vs. ChETA -10 to 0 seconds	t(36) = -0.2793	p = 0.7816
			females: eYFP vs. ChETA 0 - 10 seconds	t(36) = 2.0662	p = 0.0461*
			females: eYFP vs. ChETA 10 - 20 seconds	t(36) = -0.3514	p = 0.7274
			females: eYFP vs. ChETA 20 - 30 seconds	t(36) = 0.3180	p = 0.7523
			females: eYFP vs. ChETA 30 - 40 seconds	t(36) = 0.2057	p = 0.8381
h	binned velocity: male eYFP (n= 18); male ChETA (n =15)	two-sample t-test	males: eYFP vs. ChETA -10 to 0 seconds	t(31) = 0.8112	p = 0.4234
			males: eYFP vs. ChETA 0 - 10 seconds	t(31) = 1.0955	p = 0.2817
			males: eYFP vs. ChETA 10 - 20 seconds	t(31) = 0.4562	p = 0.6514
			males: eYFP vs. ChETA 20 - 30 seconds	t(31) = -0.4190	p = 0.6781
			males: eYFP vs. ChETA 30 - 40 seconds	t(31) = 0.3128	p = 0.7566
i	EPM delta distance travelled [ON - pre]: female eYFP (n = 20); female ChETA (n = 21); male eYFP (n = 20); male ChETA (n = 19);	three-way ANOVA	Main effect of sex	F(1,72) = 1.1883	p = 0.2793
			Main effect of opsin	F(1,72) = 0.0923	p = 0.7622
			Main effect of cohort	F(1,72) = 0.2183	p = 0.6417
			Interaction effect: sex x opsin	F(1,72) = 0.5391	p = 0.4652
			Interaction effect: sex x cohort	F(1,72) = 0.5355	p = 0.4667
			Interaction effect: treatment x cohort	F(1,72) = 0.0621	p = 0.8038
			Interaction effect: sex x opsin x cohort	F(1,72) = 0.2970	p = 0.5869
		multiple comparisons	Females: eYFP vs. ChETA	t(72) = 0.7287	p = 0.4685
			Males: eYFP vs. ChETA	t(72) = -0.3200	p = 0.7499
			eYFP: female vs male	t(72) = -0.2473	p = 0.8054
			ChETA: female vs male	t(72) = -1.2888	p = 0.2016

j	SA delta distance travelled [ON - pre]: female eYFP (n = 16); female ChETA (n = 19); male eYFP (n = 17); male ChETA (n = 16);	three-way ANOVA	Main effect of sex	F(1,60) = 4.6512	p = 0.0350*
			Main effect of opsin	F(1,60) = 0.2640	p = 0.6093
			Main effect of cohort	F(1,60) = 5.6671	p = 0.0205*
			Interaction effect: sex x opsin	F(1,60) = 3.4007	p = 0.0701
			Interaction effect: sex x cohort	F(1,60) = 0.4822	p = 0.4901
			Interaction effect: treatment x cohort	F(1,60) = 2.3172	p = 0.1332
			Interaction effect: sex x opsin x cohort	F(1,60) = 0.7234	p= 0.3984
		multiple comparisons	Females: eYFP vs. ChETA	t(60) = 0.8853	p = 0.3795
			Males: eYFP vs. ChETA	t(60) = -1.7914	p = 0.0783
			eYFP: female vs male	t(60) = -0.2231	p = 0.8242
			ChETA: female vs male	t(60) = -2.9823	p = 0.0041**
Extended Data Fig. 8					
c	MRR firing frequency: female (n = 17 cells from 6 mice); male (n = 16 cells from 6 mice)	two-sample t-test		t(31) = 2.7908	p = 0.0089**
	Female B9 vs MRR firing frequency: B9 (n = 18 cells from 9 mice); MRR (n = 17 cells from 6 mice)	two-sample t-test		t(33) = -3.4080	p = 0.0017**
	Female MRR vs DRI firing frequency: MRR (n = 18 cells from 9 mice); DRI (n = 18 cells from 9 mice)	two-sample t-test		t(33) = 3.9970	p = 0.0003***
	Female MRR vs male DRI firing frequency: female MRR (n = 18 cells from 9 mice); male DRI (n = 19 cells from 10 mice)	two-sample t-test		t(30) = 3.6563	p = 0.0010**
	Female MRR vs male B9 firing frequency: female MRR (n = 18 cells from 9 mice); male B9 (n = 15 cells from 10 mice)	two-sample t-test		t(34) = 4.9532	p < 0.0001***

Extended Data Table 2

Comprehensive summary of all statistical testing for behavioral experiments detailed in Fig. 2, Fig. 3, Extended Data Fig. 6

		Three-way ANOVA							Post hoc multiple comparisons (Holm correction)			
	Levene's test	sex	treatment	cohort	sex x treatment	sex x cohort	treatment x cohort	sex x treatment x cohort	F-YFP vs M-YFP	F-YFP vs F-ChR2	M-YFP vs M-ChR2	F-ChR2 vs M-ChR2
elevated plus maze												
time in closed	0.218	0.249	0.660	0.000	0.015	0.602	0.950	0.413	0.345	0.038	0.165	0.013
number entries open arm	0.526	0.165	0.270	0.114	0.039	0.678	0.628	0.047	0.607	0.028	0.508	0.020
distance travelled	0.145	0.279	0.762	0.642	0.465	0.467	0.804	0.587	0.805	0.469	0.750	0.202
mean velocity	0.182	0.599	0.274	0.038	0.435	0.782	0.392	0.816	0.871	0.851	0.206	0.350
time immobile	0.353	0.160	0.969	0.446	0.231	0.425	0.749	0.522	0.880	0.405	0.385	0.067
number of head dips	0.538	0.200	0.209	0.000	0.008	0.807	0.556	0.493	0.298	0.005	0.332	0.007
number of stretchings	0.055	0.031	0.000	0.335	0.000	0.311	0.833	0.046	0.130	0.000	0.661	0.000
number of groomings	0.158	0.048	0.000	0.097	0.000	0.026	0.606	0.178	0.206	0.000	0.986	0.000
time grooming	0.008	0.007	0.022	0.011	0.000	0.966	0.874	0.927	0.425	0.000	0.289	0.000
grooming duration	0.518	0.277	0.484	0.020	0.008	0.707	0.884	0.896	0.245	0.016	0.158	0.009
successive alleys												
occupancy score	0.262	0.003	0.678	0.344	0.590	0.463	0.350	0.347	0.101	0.460	0.928	0.013
time in zone 1	0.407	0.000	0.532	0.623	0.489	0.812	0.206	0.167	0.018	0.335	0.961	0.001
number entries zone 2 + 3 + 4	0.325	0.235	0.193	0.145	0.036	0.365	0.672	0.824	0.562	0.018	0.649	0.024
distance travelled	0.377	0.035	0.609	0.020	0.070	0.490	0.133	0.398	0.824	0.380	0.078	0.004
time immobile	0.398	0.004	0.318	0.026	0.249	0.516	0.400	0.348	0.212	0.874	0.116	0.003
mean velocity	0.593	0.428	0.541	0.041	0.023	0.250	0.552	0.436	0.041	0.231	0.039	0.225
number of head dips	0.780	0.004	0.796	0.202	0.049	0.991	0.103	0.502	0.589	0.090	0.237	0.001
number of stretchings	0.704	0.004	0.004	0.170	0.235	0.187	0.138	0.068	0.305	0.003	0.267	0.004
number of groomings	0.163	0.015	0.008	0.098	0.131	0.756	0.774	0.639	0.536	0.003	0.369	0.008
time grooming	0.893	0.004	0.035	0.169	0.342	0.440	0.885	0.444	0.174	0.032	0.379	0.010
grooming duration	0.370	0.401	0.595	0.982	0.607	0.336	0.391	0.936	0.423	0.999	0.539	0.852
open field												
distance travelled	0.139	0.185	0.123	0.000	0.282	0.351	0.821	0.222	0.091	0.592	0.045	0.957
mean velocity	0.899	0.902	0.936	0.004	0.167	0.511	0.283	0.546	0.372	0.387	0.220	0.230
time immobile	0.138	0.220	0.103	0.002	0.610	0.295	0.994	0.239	0.218	0.326	0.100	0.688
number of groomings	0.120	0.319	0.323	0.159	0.471	0.728	0.314	0.205	0.846	0.210	0.674	0.354
time grooming	0.385	0.929	0.580	0.046	0.850	0.285	0.339	0.968	0.855	0.615	0.546	0.975
grooming duration	0.654	0.210	0.603	0.658	0.292	0.389	0.501	0.216	0.854	0.372	0.743	0.185

all values represent *P*-values. Significant results ($P < 0.05$) are indicated in green.